HAL
open science

Data-based estimates of the ocean carbon sink variability – first results of the Surface Ocean pCO2 Mapping intercomparison (SOCOM)

Christian Rödenbeck, Dorothee C. E. Bakker, Nicolas Gruber, Yosuke Iida, Andrew R. Jacobson, Stephen D. Jones, Peter Landschützer, Nicolas Metzl, Shin-Ichiro Nakaoka, Are Olsen, et al.

To cite this version:

Christian Rödenbeck, Dorothee C. E. Bakker, Nicolas Gruber, Yosuke Iida, Andrew R. Jacobson, et al.. Data-based estimates of the ocean carbon sink variability – first results of the Surface Ocean pCO2 Mapping intercomparison (SOCOM). 2015. hal-01187676

HAL Id: hal-01187676

https://hal.science/hal-01187676v1

Preprint submitted on 7 Dec 2015

HAL is a multi-disciplinary open access archive for the deposit and dissemination of scientific research documents, whether they are published or not. The documents may come from teaching and research institutions in France or abroad, or from public or private research centers.

L'archive ouverte pluridisciplinaire **HAL**, est destinée au dépôt et à la diffusion de documents scientifiques de niveau recherche, publiés ou non, émanant des établissements d'enseignement et de recherche français ou étrangers, des laboratoires publics ou privés.

Distributed under a Creative Commons Attribution 4.0 International License

Biogeosciences Discuss., 12, 14049–14104, 2015
www.biogeosciences-discuss.net/12/14049/2015/
doi:10.5194/bgd-12-14049-2015
© Author(s) 2015. CC Attribution 3.0 License.

Biogeosciences Discussions
Open Access

This discussion paper is/has been under review for the journal Biogeosciences (BG). Please refer to the corresponding final paper in BG if available.

Data-based estimates of the ocean carbon sink variability – first results of the Surface Ocean pCO_2 Mapping intercomparison (SOCOM)

C. Rödenbeck[1], D. C. E. Bakker[2], N. Gruber[3], Y. Iida[4], A. R. Jacobson[5], S. Jones[13], P. Landschützer[3], N. Metzl[6], S. Nakaoka[7], A. Olsen[8], G.-H. Park[9], P. Peylin[10], K. B. Rodgers[11], T. P. Sasse[12], U. Schuster[13], J. D. Shutler[13], V. Valsala[14], R. Wanninkhof[15], and J. Zeng[7]

[1]Max Planck Institute for Biogeochemistry, Jena, Germany
[2]Centre for Ocean and Atmospheric Sciences, School of Environmental Sciences, University of East Anglia, Norwich, UK
[3]Institute for Biogeochemistry and Pollutant Dynamics, ETH Zürich, Zürich, Switzerland
[4]Global Environment and Marine Department, Japan Meteorological Agency, Tokyo, Japan
[5]University of Colorado and NOAA Earth System Research Laboratory, Boulder Colorado, USA
[6]Sorbonne Universités (UPMC, Univ Paris 06)-CNRS-IRD-MNHN, LOCEAN/IPSL Laboratory, Paris, France

[7]National Institute for Environmental Studies, Tsukuba, Japan
[8]Geophysical Institute, University of Bergen and Bjerknes Centre for Climate Research, Bergen, Norway
[9]East Sea Research Institute, Korea Institute of Ocean Science and Technology, Uljin, Republic of Korea
[10]Laboratoire des Sciences du Climat et de l'Environnement (LSCE), Gif sur Yvette, France
[11]AOS Program, Princeton University, NJ, USA
[12]Climate Change Research Centre, University of New South Wales, Sydney, Australia
[13]College of Life and Environmental Sciences, University of Exeter, UK
[14]Indian Institute of Tropical Meteorology, Pune, India
[15]NOAA/AOML, 4301 Rickenbacker Causeway, Miami, FL, USA

Received: 26 May 2015 – Accepted: 31 July 2015 – Published: 27 August 2015

Correspondence to: C. Rödenbeck (christian.roedenbeck@bgc-jena.mpg.de)

Published by Copernicus Publications on behalf of the European Geosciences Union.

Abstract

Using measurements of the surface-ocean CO_2 partial pressure (pCO_2) and 14 different pCO_2 mapping methods recently collated by the Surface Ocean pCO_2 Mapping intercomparison (SOCOM) initiative, variations in regional and global sea–air CO_2 fluxes have been investigated. Though the available mapping methods use widely different approaches, we find relatively consistent estimates of regional pCO_2 seasonality, in line with previous estimates. In terms of interannual variability (IAV), all mapping methods estimate the largest variations to occur in the Eastern equatorial Pacific. Despite considerable spead in the detailed variations, mapping methods with closer match to the data also tend to be more consistent with each other. Encouragingly, this includes mapping methods belonging to complementary types – taking variability either directly from the pCO_2 data or indirectly from driver data via regression. From a weighted ensemble average, we find an IAV amplitude of the global sea–air CO_2 flux of 0.31 PgC yr^{-1} (standard deviation over 1992–2009), which is larger than simulated by biogeochemical process models. On a decadal perspective, the global CO_2 uptake is estimated to have gradually increased since about 2000, with little decadal change prior to 2000. The weighted mean total ocean CO_2 sink estimated by the SOCOM ensemble is consistent within uncertainties with estimates from ocean-interior carbon data or atmospheric oxygen trends.

1 Introduction

The global ocean acts as a major sink for anthropogenic carbon, and thereby helps to slow down the human-induced warming of the Earth's climate (Stocker et al., 2013). Presently, approximately 27 % of the annually emitted carbon is taken up by the ocean (Le Quéré et al., 2015); in total 30 % of the anthropogenic carbon emitted since the industrialization of our planet has been stored by the ocean (Sabine et al., 2004; Khatiwala et al., 2013). Thus, variations in the oceanic carbon sink, in particular a possible

BGD
12, 14049–14104, 2015

decline under climate change, co-determine the future climate trajectory. In addition to this direct relevance, present-day variations in the sea–air CO_2 exchange, when related to possible driving factors, can be employed to provide information on the underlying mechanisms of ocean biogeochemistry.

Until recently, estimates of the oceanic CO_2 uptake rate and its variability were largely based on (1) ocean biogeochemical process models (see, e.g., Wanninkhof et al., 2013), (2) inverse estimates based on atmospheric CO_2 data (see Peylin et al., 2013), or (3) inverse estimates based on ocean-interior carbon data (Gloor et al., 2003, and subsequent refinements). However, while process models are useful tools to study the sensitivity of carbon fluxes to the physical and biogeochemical mechanisms that controls them, they are not specifically designed for state estimation and thus have large uncertainties if used in this way (Wanninkhof et al., 2013): though forward models can be tuned to reproduce WOCE-era transient tracer inventories, such tuning cannot be expected to enhance model skill in reproducing trends and interannual variability. Likewise, while atmospheric CO_2 inversions are able to provide useful estimates of land–air CO_2 exchange on large scales, their sea–air CO_2 flux estimates suffer from large relative errors in most parts of the ocean due to the dominance of land variability in the atmospheric signals (Peylin et al., 2013). Finally, while ocean-interior inversions offer a strong data-based constraint on the long-term flux in larger regions, they do not provide flux variability or any finer spatial detail.

A more direct quantification of the sea–air CO_2 flux is possible using measurements of the oceanic and atmospheric partial pressures of CO_2 (pCO_2) in conjunction with a parameterization of the gas transfer across the sea–air interface. Through extensive concerted community efforts, more than 10 million surface ocean pCO_2 measurements were gathered and recently compiled into the SOCATv2 (Surface Ocean Carbon Atlas version 2, Bakker et al., 2014) and the LDEOv2013 (Lamont-Doherty Earth Observatory version 2013, Takahashi et al., 2014a) databases.

Although pCO_2 data are thus available in nearly all ocean basins for several decades, observations from ships or fixed sensors can necessarily only cover a tiny fraction of

BGD
12, 14049–14104, 2015

the spatio-temporal pCO_2 field of the global surface ocean. Therefore, to obtain continuous sea–air CO_2 flux fields over larger areas or the entire ocean, interpolation methods are needed to estimate values in all the periods and areas not directly observed. Various methods have been proposed to interpolate pCO_2 data in space and time (Appendix A). They span a wide range of approaches, in particular with respect to the information sources tapped and assumptions imposed. Due to that, some methods are able to reproduce the signals in the data more closely while others are able to bridge the data-void areas/periods more effectively (Fig. 1).

These complementary characteristics of the various approaches to some degree reflect differing targets of the individual studies. Correspondingly, their strengths and weaknesses can be expected to differ depending on a considered purpose. However, this complementarity offers a great opportunity for robustness assessment, as the existence of common features in the results of mapping methods based on different principles give strong support to the estimates. In periods or areas without data, this is the only available way to assess uncertainties. Further, we can investigate the information content of the various data streams used by some methods and not used by others. It is the primary objective of the SOCOM initiative to foster such inter-method investigations. SOCOM is not meant to rank methods but to exploit the added value of their complementarity. Ultimately it aims to identify which features of the surface-ocean pCO_2 field (and consequently the sea–air CO_2 flux) can be robustly inferred from the available surface-ocean carbon data, and to provide quantitative estimates for these features, including an uncertainty assessment. These sea–air CO_2 flux estimates based on surface-ocean carbon data are then available to feed into comprehensive carbon cycle syntheses like the REgional Carbon Cycle Assessment and Processes (RECCAP) activity of the Global Carbon Project (http://www.globalcarbonproject.org/reccap/), which until recently mainly had to rely on model simulations for variability.

This paper first introduces the ensemble of data-driven pCO_2 mapping methods currently available in the SOCOM initiative (Sect. 2), and gives an overview of the estimated seasonality and interannual variability (IAV) in oceanic "biomes" (Sect. 4.1).

BGD
12, 14049–14104, 2015

As some of these pCO_2 data-driven methods have been used to assess interannual variations of global sea–air CO_2 fluxes in recent carbon budgets by the Global Carbon Project (GCP) (Le Quéré et al., 2015), we then specifically analyse the interannual variations in the sea–air CO_2 fluxes. Focus is put on the consistency between regressing and non-regressing methods, and on the amplitude of the interannual sea–air CO_2 flux variability (Sect. 4.2).

2 Mapping methods

This section provides a short overview of the principles of the various mapping approaches, and the range of particular choices taken within each method class (some methods also combine elements of several classes). Details on the individual mapping methods (referenced by labels in italics) are given in Appendix A and the references cited there. Some essential properties and technical parameters are summarized in Tables 1–3. In particular, Table 3 gives the spatial and temporal coherence scales of the adjustible degrees of freedom, determining the balance between the ability of a method to bridge data gaps and its ability to directly follow the observed signals (see table footnote *e*). Table 4 indicates which modes of pCO_2 variability are, by construction of the individual methods, estimated from the pCO_2 data information (rather than prescribed or determined in other ways). For a summary of method classes see again Fig. 1 and its caption.

2.1 Statistical interpolation

Statistical interpolation schemes fit the data to suitable auto-regressive models. The applied auto-correlation scales have either been determined from the pCO_2 data themselves (*UEA-SI*, *OceanFlux-SI*), chosen to reflect data density (*Jena-MLS*), or derived from process model simulations (*CU-SCSE*). The interpolation is either done directly

BGD
12, 14049–14104, 2015

for the pCO_2 field (*UEA-SI*, *OceanFlux-SI*, *CU-SCSE*) or indirectly for a quantity determining pCO_2 (*Jena-MLS*).

In most statistical interpolation schemes, those pixels/timesteps that are neither directly constrained by co-located data, nor indirectly constrained by sufficiently close data (within the spatial or temporal correlation scales), fall back to some "background state" or "prior", namely: the estimated mean seasonality and trend (*UEA-SI*), parametrized temperature-related variations (*Jena-MLS*), or a prescribed climatology plus a prescribed linear trend (*CU-SCSE*). The ordinary block kriging used in *OceanFlux-SI* does not use a-priori data values and interpolates the data to any distance, though the estimation uncertainty increases with interpolation distance.

2.2 Regression to external drivers

2.2.1 Linear regression

(Multi-)linear regression (*AOML-EMP*, *UEx-MLR*, *JMA-MLR*) expresses pCO_2 as a linear combination of a set of one or more driving variables (such as Sea Surface Temperature (SST), Sea Surface Salinity (SSS), Mixed-layer depth (MLD), Chlorophyll *a*, etc.), and adjusts their multipliers as to best match the observations. The calculation is done separately for each of a set of spatio-temporal domains. Individual implementations differ in the set of chosen driver variables, as well as in the choice of spatio-temporal domains over which the same adjustable multipliers are used.

2.2.2 Non-linear regression

The forms of non-linear regression technique currently applied to map the sea surface pCO_2 are self–organizing maps (SOM) (*NIES-SOM*) and feed-forward networks (FFN) (*NIES-NN*, *CARBONES-NN*), as well as combinations of SOM and FFN (*ETH-SOMFFN*) or SOM and linear regression (*UNSW-SOMLO*).

BGD
12, 14049–14104, 2015

– Self-organizing maps (SOM) project (multi-dimensional) driver variables to a two-dimensional discrete space of clusters ("neuron cells"). Observed pCO_2 values are then assigned to the clusters according to their associated driver variable values. With this information, spatio-temporal pCO_2 maps are created by finding neuron cells with similar driver variable values for any given location/timestep, and using the associated pCO_2 value there.

– Feed-forward networks (FFN) establish a statistical non-linear relationship between a set of driver variables and pCO_2 observations (training), and apply this relationship to continuous fields of the driver variables to create a continuous pCO_2 map (prediction).

As for linear regression, the individual implementations differ in the set of chosen physical or biogeochemical driver variables (SST, SSS, MLD, Chl *a*, etc.). Different choices have also been made concerning spatialization: While some implementations use independent neural networks within predefined spatial or spatio-temporal regions, others use one global network but add spatial or temporal coordinate variables to the set of drivers.

Non-linear regression methods represent pCO_2-driver relationships in a more flexible manner than linear regressions, however the non-linear extrapolation into data-sparse regions involves the risk of becoming unstable. FFNs have the advantage that they produce a continuous number of outputs, while the discrete SOM output may involve spatial discontinuity. However, SOMs have the advantage that no a-priori knowledge or empirical descriptions between drivers and pCO_2 data are needed (Telszewski et al., 2009).

2.3 Model-based regression and tuning

Biogeochemical ocean process models have been used in various ways:

– Modelled pCO_2 fields have been split into different time scales (seasonality, interannual variations) and scaled as to optimally match the pCO_2 data (*PU-MCMC*).

BGD
12, 14049–14104, 2015

– Parameters or initial fields in the model itself are tuned as to optimally match the pCO_2 data (*NIES-OTTM*).

3 Analysis methods

3.1 Ensemble collection

The pCO_2 fields estimated by the various methods were regridded by each provider to a resolution of 1° latitude × 1° longitude and monthly time steps, preferably by averaging (if the original resolution is higher) or sub-sampling (if the original resolution is lower). Also a sea-mask (map of covered ocean area, possibly fractional) was requested from each provider. All subsequent processing was done by common scripts.

3.2 Spatial gap filling

Most methods do not cover the entire ocean surface (see Fig. A6). In particular, coastal areas or the Arctic are excluded in many methods. Some methods depending on satellite-derived Chlorophyll *a* input data exclude some high-latitude areas during the dark season. *OceanFlux-SI* misses all locations/months where the satellite-derived SST input data are invalid. *UEx-MLR* has occasional invalid pixels due to numerical reasons.

These invalid pixels would pose severe problems to the ensemble analysis because (1) spatial averages (Sect. 3.3) would not extend over the same area, causing spurious differences between the methods, and (2) the calculated sea–air CO_2 fluxes (Sect. 3.6) would miss parts of the ocean. Restricting the comparison to the common ocean surface would only partially solve (1) and not solve (2).

Therefore, we filled any pixels in the pCO_2 maps that are not covered by the considered mapping method (according to its sea mask or its value being outside $0 < pCO_2 < 10^6$ µatm) but are ocean (according to bathymetry taken from the ETOPO surface elevation data U. S. Department Commerce, 2006) by a common standard

BGD
12, 14049–14104, 2015

pCO_2 field. This standard field has been derived from the climatology by Takahashi et al. (2014b) plus the atmospheric pCO_2 increase[1]. The filled pixels do not change the results strongly compared to signal size.

3.3 Biome averages

In this overview of the ensemble of results, we consider time series of pCO_2 averaged over the 17 biomes of Fay and McKinley (2014) (Fig. 2, Table 5). We use the time-independent "mean biomes", such that no spurious common variability can be induced from changing averaging domains. These biomes were chosen as they were derived from coherence in sea surface temperature (SST), spring/summer chlorophyll *a* concentrations (Chl *a*), ice fraction, and maximum mixed layer depth, and thus may reflect areas of relatively coherent biogeochemical behaviour better than previously used "rectangular" regions (e.g., RECCAP, TransCom). To filter for interannual variations (IAV), we consider 12 month running means.

3.4 Time periods

Results are plotted over the respective valid period of each method. Statistical analyses are restricted to the 1992–2009 period, when results of most mapping methods are available, and when the data coverage is relatively good (this refers in particular to the Equatorial Pacific).

[1]The atmospheric pCO_2 increase is derived from a 12 month running mean of pCO_2^{atm} minus its mean in 2005, the year of the Takahashi et al. (2014b) climatology. pCO_2^{atm} is derived from the atmospheric CO_2 mixing ratio taken from an inversion of atmospheric CO_2 observations as in Rödenbeck et al. (2013).

BGD
12, 14049–14104, 2015

3.5 Diagnostics

As a 1st order performance diagnostic, we compare the mapping results to the monthly observed values in the SOCATv2 gridded product (Sabine et al., 2013; Bakker et al., 2014). In these comparisons, the averages over biomes or biomes/years are taken only over those pixels/months that are covered by data (and with at least 400 m water depth to avoid coastal data; these coastal data may otherwise dominate the diagnostics as the methods do not take the special environment along the coasts into account)[2]. We consider time series of such selective averages of the pCO_2 maps themselves as well as of their difference to the data.

As an overall measure of the mismatch between a given mapping product and the data with respect to interannual variations in a given biome, we use the amplitude M^{iav} (temporal standard deviation[3]) of the average difference between map and data (averages over biomes and years, again restricted to data-covered open-ocean pixels/months). To be able to set these mismatch amplitudes into perspective, we similarly determine the mismatch amplitude $M^{iav}_{benchmark}$ of "benchmark" fields where any oceanic IAV has been removed[4]. We then obtain a relative IAV mismatch for the given method

[2]Spatial averages are further restricted to the valid area of each method. This may slightly favor methods with less surface coverage, because fewer data pixels are then included in the mismatch.

[3]The temporal standard deviation is calculated over the 1992–2009 analysis period. If a method does not cover all this analysis period, statistics are calculated for a correspondingly shorter period (Table 2), despite the slight inconsistency due to IAV.

[4]The benchmark maps have been created from the mean seasonal cycle of the respective original maps. As the missing pCO_2 increase would cause unduly large mismatches between the benchmark and the data, we added the year-to-year atmospheric pCO_2 increase, which is suitable as it has negligible interannual variations compared to oceanic pCO_2. The increase has been computed from atmospheric CO_2 data as described in Footnote 1.

BGD
12, 14049–14104, 2015

and biome as

$$R^{\mathrm{iav}} = \frac{M^{\mathrm{iav}}}{M^{\mathrm{iav}}_{\mathrm{benchmark}}} \cdot 100\,\% \tag{1}$$

It states by how much an estimate fits the data better due to its interannual variations, compared to a state of "no knowledge" about IAV. Alternatively, Eq. (1) can be seen as a normalization of the IAV mismatch to signal size: As the benchmark fields do not contain any IAV, their mismatch amplitudes $M^{\mathrm{iav}}_{\mathrm{benchmark}}$ reflect the IAV in the data (influences of variations in data density will affect M^{iav} and $M^{\mathrm{iav}}_{\mathrm{benchmark}}$ in similar ways). Calculating the benchmark from each product's own seasonal cycle ensures a criterion comparable between the mapping methods (though the seasonal cycles are quite similar for all methods anyway, see Sect. 4.1.1 below).

It is difficult to decide which R^{iav} values can be regarded as sufficient for IAV to be represented in a given map. For this paper, we present all IAV results that manage to stay below 75 %. This is an ample threshold, but in the light of possible ambiguities in the R^{iav} calculation we preferred it over a stricter selection. To nevertheless make the likely range more visible, we de-weight results with higher R^{iav} by smaller line thickness in all IAV plots.

To verify the robustness of the selection criterion, IAV mismatch diagnostics have also been calculated from the LDEOv2013 database (Takahashi et al., 2014a) (monthly binned), which is used as data source by some mapping methods. LDEOv2013 shares large parts of data points with SOCATv2. Mismatch values are slightly different depending on database, but qualitatively consistent.

3.6 Sea–air flux calculation

Sea–air CO_2 flux fields f have been calculated from the pCO_2 fields by

$$f = k\varrho L \left(pCO_2 - pCO_2{}^{\mathrm{atm}}\right) \tag{2}$$

BGD
12, 14049–14104, 2015

with piston velocity k (employing the widely used quadratic dependence on wind speed as in Wanninkhof, 1992, reduced to 10 % over ice as in Takahashi et al., 2009), water density ϱ, CO_2 solubility L, and atmospheric CO_2 partial pressure pCO_2^{atm}. The values of these auxiliary fields have been calculated from various data sets (e.g., NCEP wind speeds from Kalnay et al., 1996, OAFlux SSTs and ice cover from Yu and Weller, 2007) as in Rödenbeck et al. (2013, see there for details) and used identically for all mapping methods, i.e., the uncertainties in the flux parameterization do not enter the comparison considered here.

Interannual flux variations are again calculated as 12 month running means. Their amplitude A^{iav} is measured as temporal standard deviation of the yearly flux over the 1992–2009 analysis period. From the amplitudes A_i^{iav} of the individual mapping methods, we calculate an ensemble mean inversely weighted by the relative IAV mismatches R_i^{iav} (for methods with $R_i^{iav} < 75\,\%$)

$$\overline{A^{iav}} = \frac{\sum_{i=1}^{n} A_i^{iav}/R_i^{iav}}{\sum_{i=1}^{n} 1/R_i^{iav}} \tag{3}$$

Methods not covering the full analysis period are discarded here as there would be significant spurious changes in the amplitude if any of the El Niño anomalies in 1992 or 1997 was not included.

4 Results and discussion

We first provide an overview on the estimated seasonal and interannual variations in oceanic biomes (Sect. 4.1), and the ability to estimate them from pCO_2 data and available mapping methods. We then discuss interannual variations in the sea–air CO_2 flux in more detail (Sect. 4.2).

BGD
12, 14049–14104, 2015

4.1 Biome-average pCO_2 time series

4.1.1 Seasonality

As introductory example, we first consider surface ocean pCO_2 averaged over the North Atlantic Subtropical Permanently Stratified biome, which belongs to the relatively well observed regions and shows a pronounced seasonal cycle in pCO_2 (Schuster et al., 2013). Figure 3a shows monthly pCO_2 time series from the whole ensemble. For clarity of details, three arbitrary years have been selected. The results of the mapping methods generally agree with each other in terms of the mean and the seasonal cycle to within about 10 µatm.

Panel b compares the mapping results to the SOCATv2 monthly observations. To this end, mapping results have been averaged only over those locations/times where data exist. As these are the locations/times where (most of) the estimates are directly constrained, the mapping results generally follow the data closely, and the ensemble spread is often smaller than in panel a. In some months (e.g., Sept. 2003 or July 2004) these selective averages deviate considerably from the whole-biome average, likely reflecting spatial sampling biases in the presence of spatial pCO_2 gradients. In such months, the ensemble spread tends to be higher than in months less affected by sampling biases.

To objectively compare our results to the in-situ data, we calculate the average difference between the mapped pCO_2 (at the data location) and the SOCATv2 monthly values (panel c). In general, differences of the monthly values lie within about ±10 µatm. *NIES-OTTM* deviates farther, likely because this approach is strongly determined by the modelled seasonal cycle and thus does not follow the data more closely.

Time series for the complete set of biomes are given in the Appendix. In terms of seasonality, the mapping methods show similar phasing and amplitude in almost all extra-tropical biomes (Fig. A1), with few exceptions mainly in the North Atlantic Sub-

BGD
12, 14049–14104, 2015

polar Seasonally Stratified biome[5] and the Southern Ocean. The spread in the North Atlantic is somewhat surprising given the relatively good data coverage. Methods agree on smaller seasonal amplitude in the tropics, though substantial differences in amplitude and phase exist.

4.1.2 Interannual variability (East Pacific Equatorial biome)

Interannual variability is exemplified with the East Pacific Equatorial biome, which is also relatively well observed, and features large coherent interannual variations in pCO_2 associated with the ENSO cycle (e.g., Feely et al., 1999). Figure 4a shows the results of those mapping methods with IAV mismatches (R^{iav}, Sect. 3.5) of at most 75 % of signal size. This selection has been done because, in contrast to seasonality, interannual signals in the data turn out not to be represented in all mapping methods; thus the full ensemble (Appendix Fig. A2 panel "Biome 6") would highly overestimate the uncertainty of IAV. All the 8 selected mapping methods consistently show a reduction in ocean surface pCO_2 during El Niño conditions (1987, 1992, strong El Niño 1997/98, weak El Niño's also 2002, 2006, 2009/10), though partially with different amplitudes (see Sect. 4.2.1 for the particularly low amplitude of *UEA-SI*). Methods regressing pCO_2 against external drivers (*JMA-MLR*, *UNSW-SOMLO*, *NIES-SOM*, *ETH-SOMFFN*) tend to show mutually similar time variations also on the finer 1–2 year time scale (e.g., 2008–2009), while statistical interpolation methods (*UEA-SI*, *Jena-MLS*) may show different finer-scale features. Despite this biome-wide difference, averages at data-constrained pixels only (Fig. 4b) mostly are much more consistent between methods. This is expected as this selective average excludes all the gap-filled pixels

[5] *NIES-OTTM* shows a seasonal cycle opposite to the other methods, a behaviour present in many biogeochemical process models in high latitudes (Valsala and Maksyutov, 2010; Schuster et al., 2013). However, also the other methods strongly differ in their seasonal cycle amplitude in the North Atlantic Subpolar Seasonally Stratified biome, likely a result of the sparse data coverage here, but maybe also of the large extension of the biome.

BGD
12, 14049–14104, 2015

where values naturally depend much more on the applied mapping method. Most strikingly, in the data-poor periods up to 1988 and from 2009 onwards (see data density in Fig. A5 panel "Biome 6"), regression and interpolation methods (as far as they cover these periods) strongly differ in the whole-biome average (panel a), while they closely agree at the data-covered pixels (panel b). This illustrates that the statistical interpolation methods solely rely on the pCO_2 data constraint while regression methods bridge data gaps as their variability originates from the driver data that are available throughout time. In the more data-rich periods (about 1992–2008 in this biome), interpolation and regression methods do agree in many features even in the whole-biome average (panel a). Due to the complementary origin of the variability in these method classes (Fig. 1), this agreement confirms that, at least in this biome, (1) sufficient interannual information is contained in the available pCO_2 observations (in the more densely sampled period), and (2) the signals provided through the driver data of the regression methods largely capture the essential modes of interannual pCO_2 variability.

Note that the selective average over data-covered pixels (panel b) also leads to temporal features very different from the full average (e.g., the peak in 2001), revealing sampling biases that alias seasonal variations and spatial gradients into the yearly/spatial average due to not fully representative sampling. These sampling biases pose the most prominent challenge to all the mapping methods.

Panel c shows the average difference between the interpolated pCO_2 fields and the SOCATv2 monthly data set, reflecting the mismatch of mean, trend, and interannual variations (the sampling biases mentioned before should largely cancel out in this difference). Most mapping methods have a temporal mean mismatch (bias) of less than a few µatm. The year-to-year mismatches are of different magnitudes for the individual mapping methods[6]. Though the estimated interannual features can only be trusted if the year-to-year mismatches are small (necessary condition), small year-to-year mismatches are not yet a sufficient condition for correct interannual variations: Even if the

[6]Note that the larger mismatches in 2009/10 occur in a period of very few data points and may not be representative.

BGD
12, 14049–14104, 2015

available data points are fit well, the extrapolation to data-void areas can be wrong ("over-fitting", see more discussion in Sect. 4.2 below). Therefore, we stress that the mismatch amplitudes are not meant to represent a detailed ranking of quality of the methods. Nevertheless, we take it as an encouraging finding that mapping methods with smaller IAV mismatch (e.g., passing the more strict relative IAV mismatch criterion of $R^{iav} < 30\,\%$ [*Jena-MLS*, *ETH-SOMFFN*]) are also closer to each other in the whole-biome average (panel a). Even this stricter selection comprises methods regressing or not regressing pCO_2 against external drivers, i.e., complementary ways of extrapolating to data-void areas/periods (Fig. 1, Table 3 table footnote *e*). This reinforces conclusions (1) and (2) above and confirms that meaningful interannual estimates can be achieved from the available pCO_2 data and mapping methods in the Equatorial Pacific.

4.1.3 Interannual variability (other biomes)

Considering now all the biomes, all mapping methods agree that the East Pacific Equatorial biome considered before (Sect. 4.1.2) has the largest interannual variability (Fig. A2). The other biomes have much less interannual variability, leaving the rising trend (similar to the atmospheric CO_2 increase) as the most prominent interannual feature. There is one mapping method (*NIES-OTTM*) without a trend, a feature not however supported by the data (see large data mismatch with systematic trend in Fig. A3). Except for the West and East Pacific Equatorial biomes, the small year-to-year variations around the rising trend are not generally consistent between the mapping methods (ensemble spread similar or larger than the variations themselves).

Overall, mean mismatches (biases) are on the order of 3–4 µatm in all biomes (Fig. A3). As the mismatches do not consistently rise or fall over time, they confirm the estimated pCO_2 trends (except for *NIES-OTTM* that does not have the rising trend in pCO_2). The year-to-year mismatches have amplitudes of 3–4 µatm in some methods, but also mismatches as large or larger than the interannual variations for other methods ($R^{iav} > 75\,\%$, dashed lines). Except for the North Atlantic Subtropical Sea-

BGD
12, 14049–14104, 2015

sonally Stratified biome, each ocean region has at least some mapping methods with relative IAV mismatch below 60 or even 30 %, including both interpolation methods as well as linear and non-linear regressions. Methods tying IAV to process model simulations (*PU-MCMC*, *NIES-OTTM*) often have large relative IAV mismatches, except for *PU-MCMC* in the Northern Pacific biomes.

4.2 Sea–air CO_2 flux variability

In order to link the estimated pCO_2 variability to variability of sea–air CO_2 exchange as considered for the Global Carbon Project (GCP) (Le Quéré et al., 2015), we calculated sea–air CO_2 fluxes f, using the same gas exchange formulation for each mapping method (Sect. 3.6).

4.2.1 The East Pacific Equatorial biome

We first consider again the East Pacific Equatorial biome identified above as the biome with the largest interannual variability. Figure 5a provides its sea–air CO_2 fluxes estimated by 8 selected mapping methods (having relative IAV mismatch $R^{iav} < 75\,\%$ for biome-averaged pCO_2). The year-to-year flux variations are mainly driven by the pCO_2 variability (compare to Fig. 4a). Again, interannual features are largely similar between the mapping methods in this biome, but differ in their amplitudes (Fig. 5b). There is some tendency that the mapping methods with smaller IAV mismatch show larger interannual amplitudes. Strikingly low interannual variability is found in *UEA-SI*, while fitting the data with $R^{iav} = 52\,\%$ better than various other methods. This method moves away from the estimated mean seasonality only in the close vicinity of the data points, as justified by the short auto-correlation lengths of near-simultaneous pCO_2 levels found in the pCO_2 data (Jones et al., 2012). It thus gives a lower bound of IAV secured by the data information (Jones et al., 2015). As interannual features can be assumed to be more spatially coherent than features on the time scale of ship cruises (especially in the Equatorial Pacific), the higher IAV amplitudes are likely.

BGD
12, 14049–14104, 2015

4.2.2 The global ocean

Figure 5c provides global sea–air CO_2 fluxes estimated by 10 selected mapping methods (having relative IAV mismatch $R^{iav} < 75\,\%$ for global pCO_2). These mapping methods mostly agree in their decadal variations, with a pronounced decadal increase in ocean CO_2 uptake after the year 2000, preceded by a period of little decadal change or rather decreasing uptake. There is less agreement in the sub-decadal variations, despite the much closer mutual agreement of the same mapping methods in the well-constrained East Pacific Equatorial biome (Fig. 5a). This lower agreement reflects the more uncertain flux contributions from the poorly data-constrained areas. For example, the larger sub-decadal variations by *Jena-MLS* to large part originate from the South Pacific Subtropical Permanently Stratified biome (Fig. A4 panel "Biome 7"), which is a data-poor region and therefore recieves spurious variability from the Equatorial Pacific extrapolated too far south[7]; indeed, the amplitude of the variations reduces with shorter latitudinal extrapolation radius (latitudinal a-priori correlation length, Sect. 3.3 of Rödenbeck et al., 2014).

Despite these differences in the detailed variations, the amplitude of global flux IAV (Sect. 3.6) is relatively consistent (panel d). The global weighted ensemble mean $\overline{A^{iav}}$ (Eq. 3) is 0.31 $PgC\,yr^{-1}$ (horizontal line in panel d). Many biogeochemical process models have less variability than that (mean of 0.20 $PgC\,yr^{-1}$ in Le Quéré et al., 2015) and thus likely underestimate IAV in the ocean carbon sink (compare Séférian et al., 2014; Turi et al., 2014). Inverse estimates based on atmospheric CO_2 data show both larger and smaller oceanic IAV (Peylin et al., 2013), reflecting that they can constrain land variability but less so ocean variability.

[7] Another contributor of *Jena-MLS* variability is the Pacific sector of Biome 16. In the Southern Ocean, essentially only two areas (South of New Zealand and South-West of Patagonia, respectively) are data-covered for multiple years, such that signals from there are extrapolated into their data-void surroundings.

BGD
12, 14049–14104, 2015

Though the primary strength of the pCO_2 constraint lies in its information on temporal variations and smaller-scale spatial variations, we also consider the long-term mean global sea–air CO_2 exchange. The total mean flux (comprising both uptake induced by anthropogenic atmospheric CO_2 rise and natural river-induced outgassing) estimated by the different methods ranges between −1.36 and −1.96 PgC yr^{-1} (for the 1992–2009 analysis period), with a weighted ensemble mean (analogous to Eq. 3 but using the inverse mean pCO_2 bias as weights) of −1.75 PgC yr^{-1}. This is consistent within uncertainties with the independent estimate from inverting ocean-interior carbon data of −1.7 PgC yr^{-1} (Gruber et al., 2009) nominally for 1995. Subtracting a river-carbon induced outgassing flux of 0.45 PgC yr^{-1} (Jacobson et al., 2007), the ensemble mean corresponds to an anthropogenic CO_2 uptake of −2.2 PgC yr^{-1}. This is again consistent within uncertainties with the estimate from the globally integrative constraint by the atmospheric O_2 and CO_2 trends of -2.2 ± 0.6 PgC yr^{-1} given by Manning and Keeling (2006) for the slightly different 1993–2003 period.

5 Conclusions

Measurements of surface-ocean pCO_2, mapped into continuous space-time fields, offer a much more direct way to quantify sea–air CO_2 fluxes and their variations than previously available approaches (model simulations, atmospheric inversions, ocean-interior inversions). Taking advantage of an ensemble of 14 partially complementary surface-ocean pCO_2 mapping methods recently collated by the SOCOM initiative, we analysed sea–air CO_2 flux variability globally and for a subdivision of the ocean into 17 biomes (Fay and McKinley, 2014). This study has found that:

- Surface-ocean pCO_2 data together with mapping methods constrain the seasonality of regional pCO_2 essentially in all ocean biomes (mostly within 10 µatm).
- Interannual variations of regional pCO_2 are constrained at least in the more densely observed ocean regions (tropical Pacific, parts of the Northern temperate

BGD
12, 14049–14104, 2015

Pacific and Atlantic). The tropical Pacific is consistently estimated as the biome with the largest interannual variations, with reduced CO_2 uptake during El Niño periods. The global CO_2 uptake is estimated to have gradually increased since about 2000, with little decadal change prior to 2000.

- Interannual variations in the global sea–air CO_2 flux are estimated to have an amplitude of 0.31 $PgC\,yr^{-1}$ (average across mapping methods weighted according to IAV mismatch). Therefore most biogeochemical process models appear to significantly underestimate this variability (Le Quéré et al., 2015, quote a model-derived amplitude variation of 0.2 $PgC\,yr^{-1}$).

- Though the primary strength of the pCO_2 constraint lies in its information on temporal variations and smaller-scale spatial variations, the estimated net integrated global sea–air CO_2 flux of $-1.75\,PgC\,yr^{-1}$ (weighted ensemble mean) is consistent within uncertainties with the independent estimates based on inverting ocean-interior carbon data and on atmospheric O_2 and CO_2 trends.

The present results also adumbrate the wealth of options to further exploit the spatio-temporal pCO_2 mapping results collated within the SOCOM initiative. Agreement between complementary mapping methods taking variability either from driver data or directly from pCO_2 data (Fig. 1), as found here for the interannual variations in the tropical Pacific, lends great support to the estimated features, as it shows consistency between different information sources; such features should therefore be identified and preferentially be used for biogeochemical interpretation in forthcoming studies. Conclusions from the SOCOM ensemble should always take into consideration suitable performance diagnostics, which weight or select mapping results for their suitability in a given purpose. While the mismatch to data used as diagnostics here provides a necessary selection criterion, however, sufficient conditions for judging reliability of the considered features need to be developed in future studies (e.g., by testing the power of the mapping methods to reconstruct modelled pCO_2 fields from pseudo data subsampled as the real data). The intercomparison may serve to stimulate and guide the

BGD
12, 14049–14104, 2015

further development of pCO_2 mapping methods. SOCOM welcomes further members contributing estimates of the spatio-temporal pCO_2 field or the sea–air CO_2 flux based on surface-ocean carbon data.

Appendix A:

A1 "*UEA-SI*" (Statistical interpolation)

Method description: The approach combines temporal interpolation through curve fitting (1–4 seasonal harmonics and a linear trend) (Masarie and Tans, 1995; Schuster et al., 2009) and spatial interpolation using the concept of spatial de-correlation lengths, or a "radius of influence", interpolating data based on the likely similarity between spatially separated points (Cressman, 1959; Levitus, 1982). In addition, cubic spline fitting is used to move away from the fitted mean seasonal cycle to incorporate interannual variations where data points exist. The de-correlation scales applied in the interpolation are determined from the auto-correlation characteristics of the pCO_2 data along ship-tracks or in time (Jones et al., 2012).

Main intention/focus: To produce a pCO_2 data set for various uses. To quantify the impact of modes of climate variability on pCO_2 and air–sea fluxes. The chosen approach departs from other methods through its purely statistical approach; it does not use any other data sources than pCO_2.

Documentation: Jones et al. (2015).

Contact: Steve Jones.

A2 "*OceanFlux-SI*" (ESA STSE OceanFlux greenhouse gases)

Method description: The in-situ pCO_2 data within SOCAT are first corrected to a common satellite derived temperature dataset using an isochemical temperature dependence. This creates an in-situ dataset with a common SST reference. Each in-situ datapoint is then corrected to the year 2010 by assuming a trend of $1.5\,\mu atm\,yr^{-1}$.

BGD
12, 14049–14104, 2015

The data are then binned into a monthly $1^\circ \times 1^\circ$ format. These monthly binned data are kriged to produce a spatially complete dataset (Goddijn-Murphy et al., 2015). We finally generate an interannual time series by (1) cyclically using this climatological dataset over time, (2) adding a prescribed trend of $1.5\,\mu\text{atm}\,\text{yr}^{-1}$ in $p\text{CO}_2$, and (3) correcting the $p\text{CO}_2$ values according to the difference between the climatological SST and the actual satellite-derived SST at each time and location (Shutler et al., 2015).

Main intention/focus: Produce a spatially complete monthly climatology of $p\text{CO}_2$ data for 2010 that uses a consistent temperature dataset which is valid at a consistent depth in the water.

Documentation: Goddijn-Murphy et al. (2015) (monthly climatology), Shutler et al. (2015) (interannual variations).

Contact: Jamie Shutler.

A3 "*Jena-MLS*" (Data-driven mixed-layer scheme)

Method description: The mixed-layer scheme is a data-driven interpolation scheme, primarily based on $p\text{CO}_2$ observations but also compatible with the dynamics of mixed-layer carbon content. Firstly, the sea–air CO_2 fluxes and the $p\text{CO}_2$ field are linked to the spatio-temporal field of ocean-internal carbon sources/sinks through parametrizations of sea–air gas exchange, solubility, and carbonate chemistry, as well as a mixed-layer DIC budget equation. Then, the ocean-internal carbon sources/sinks are adjusted to optimally fit the $p\text{CO}_2$ field to the $p\text{CO}_2$ observations (in the present version: SOCATv2). Spatio-temporal interpolation is achieved by Bayesian a-priori smoothness constraints with prescribed spatial and temporal de-correlation scales; temporal interpolation also results from the inherent relaxation time scales of the mixed-layer carbon budget. Though the process parametrizations are driven by SST, wind speed, MLD climatology, Alk climatology, and some auxiliary variables, this external variability only determines features not constrained by the $p\text{CO}_2$ observations (e.g., day-to-day variations, or variability in data-void areas/periods), while the estimated $p\text{CO}_2$ field in well-

BGD
12, 14049–14104, 2015

constrained areas/periods is only determined by the observed signals (no regression against drivers).

Main intention/focus: Global CO_2 flux field product primarily based on observations only, with a focus on flux variability, also to be applied as ocean prior in atmospheric CO_2 inversion (in particular the Jena inversion, Rödenbeck, 2005). The mixed-layer scheme has been chosen because it can be extended to link carbon variability to further observables (mixed-layer PO_4, atmospheric O_2), for using these as additional independent data constraints.

Documentation: Rödenbeck et al. (2013) (method description and seasonality); Rödenbeck et al. (2014) (interannual variations and link to oxygen).

Contact: Christian Rödenbeck.

A4 "*CU-SCSE*" (Surface Carbon State Estimation)

Method description: The Surface Carbon State Estimate (SCSE v1.0, Jacobson et al., 2015) is a Kalman filter interpolation scheme for mapping pCO_2 over the global ocean during the entire period for which SOCAT point observations are available. It is designed to provide a statistically well-characterized prior estimate to an atmospheric CO_2 analysis like CarbonTracker. SCSE tracks the time-varying magnitudes of a set of basis functions, determined as an optimal difference from a reference state composed of the Takahashi et al. (2009) pCO_2 climatology for year 2000 plus a 1.5 $\mu atm\,yr^{-1}$ global trend. Uncertainties are explicitly characterized by a full-rank posterior covariance matrix, which can then be used to produce realistic error estimates for arbitrary spatial domains. SCSE is a gridded estimation scheme that tracks pCO_2 for each $1^\circ \times 1^\circ$ grid cell, but its effective spatial resolution is controlled by the number of basis functions used within each of 10 defined ocean basins. The number of basis functions used within each basin varies with time and is determined by the number of available observations. This is intended to allow higher resolution at times and places where there are more pCO_2 measurements. The basis functions include empirical orthogonal functions (EOFs) of pCO_2 from a set of CMIP5 ocean carbon cycle simulations, intended to rep-

BGD
12, 14049–14104, 2015

resent the within- and across-model variations of climatology, trends, and variability on inter-annual to decadal time scales. They are assigned widely different relaxation time scales (3 months – 5 years) as determined by the EOF analysis.

Main intention/focus:

Documentation: Jacobson et al. (2015).

Contact: Andy Jacobson.

A5 "*AOML-EMP*" (Diagnostic model using empirical relationships)

Method description: AOML-EMP uses empirical relationships between surface-ocean pCO_2 and SST, trained based on sub-annual variations in the Takahashi pCO_2 climatology and the associated climatological SST values. These relationships are then applied to interannually varying SST (using the NOAA optimal interpolation SST product www.ncdc.noaa.gov/oisst). The original analysis of Park et al. (2010a) does not implicitly include the effect of rising atmospheric CO_2 levels. In the modified Park et al. analysis presented in Le Quéré et al. (2015) the effect of increasing atmospheric CO_2 on the surface ocean is simulated by applying the output of the "CO_2-only" run of NCAR CCSM-3 model (National Center for Atmospheric Research's Community Climate System Model Version 3) to each grid cell over the time period. The sub-decadal variability is the same for each approach as they are based on the same pCO_2 mapping. The decadal trend of CO_2 flux calculated from the original *AOML-EMP* approach shows a slight decrease in uptake while the modified approach shows an increase in uptake that is attributed to a negative feedback in CO_2 uptake due to ocean warming that is overwhelmed by increased anthropogenic CO_2 uptake.

Main intention/focus: Data-driven global CO_2 flux product.

Documentation: Park et al. (2010a, b).

Contact: Geun-Ha Park.

BGD
12, 14049–14104, 2015

A6 "*UEx-MLR*"

Method description: Multi-parameter regression in 12 separate ocean regions (RECCAP regions, see http://www.globalcarbonproject.org/global/pdf/RECCAP_Soft_%20Protocol.v4.pdf and Fig. 1 in Schuster et al., 2013) from 1990 to 2012. Main data stream used as constraint: SOCATv2 gridded product (Sabine et al., 2013) plus additional recent gridded data (all on 1° latitude by 1° longitude by 1 month). Driver variables used: SST, Mixed layer depth, chlorophyll *a*, atmospheric pCO_2.

Main intention/focus: Seasonal through interannual variability of the sea–air CO_2 flux.

Documentation: Schuster et al. (2013) (RECCAP).

Contact: Ute Schuster.

A7 "*JMA-MLR*"

Method description: The global ocean was divided into 44 sub-regions based on the features of observed pCO_2 and SST/SSS/Chl *a* variability and then optimal equations for estimating pCO_2 in the sub-regions were derived from multiple regressions using SST, SSS and Chl *a* as independent variables. Rather than using time as independent variable, secular trends of pCO_2 (for wider biomes than the sub-regions) were evaluated separately from multiple regressions, subtracted from the data, and re-added to the pCO_2 map. Observed pCO_2, SST and SSS in SOCATv2 and satellite Chl *a* (SeaWiFS and MODIS/Aqua: http://oceancolor.gsfc.nasa.gov; before 1997, the climatology of satellite Chlorophyll *a* data are used) are used to derive equations and analytical SST (MGDSST: Kurihara et al., 2006), SSS (MOVE/MRI.COM-G: Usui et al., 2006) and the same Chl *a* data mentioned above are used to reconstruct the pCO_2 fields.

Main intention/focus: To map global pCO_2 and CO_2 flux field based on surface observation data and evaluate the interannual variability and long-term trend of global ocean CO_2 uptake. The merits of using simple multiple regression analysis for estimating pCO_2 include its possibility to give oceanographic explanations for the pCO_2 variability.

BGD
12, 14049–14104, 2015

Documentation: Iida et al. (2015) (method description and trend analysis).
Contact: Yosuke Iida.

A8 "*UNSW-SOMLO*" (Self-organizing multiple-linear output)

Method description: In this approach we couple a neural network clustering algorithm with a multiple linear regression (MLR) to diagnose monthly ocean surface pCO_2 distributions from 1998 through to 2011. The algorithm first captures larger-scale ocean dynamics by a data-based clustering of the grid cells into "biogeochemical fingerprints" using a self-organizing map (SOM). The SOM approach utilizes the SOCATv2 gridded pCO_2 product along with co-located SST, SSS, Chl *a*, MLD, and geographical information (*n* vector) to iteratively cluster the dataset into a set of 196 neurons (the spatial domains of which we refer to as biogeochemical fingerprints). Within each neuron, MLRs are then derived between pCO_2 and the optimal set of sea-surface temperature/salinity/Chl *a*, MLD, and atmospheric xCO_2. Thus, each MLR can be thought of as a local-scale optimizer that follows the global non-linear optimization analysis performed by the SOM. To predict pCO_2 using any independent set of driver data, a similarity measure is first used to determine which neuron best represents the driver data values, then the pCO_2 value is predicted using the regression parameters established with training data of that neuron. We call this approach SOMLO: self-organizing multiple linear output.

Main intention/focus: To diagnose monthly ocean surface pCO_2 distributions and air–sea CO_2 fluxes from 1998 through to 2011, and to advance our understanding of seasonal to inter-annual variability.

Documentation: Sasse et al. (2013).
Contact: Tristan Sasse.

BGD
12, 14049–14104, 2015

A9 "*ETH-SOMFFN*" (a combined 2-step neural network approach)

Method description: As a first step, a self-organizing map (based on climatological pCO_2, SST, SSS, MLD, and Chl *a*) is used to cluster the global ocean into biogeochemical provinces. Within each province, a feed-forward network is then used to reconstruct the non-linear relationship between drivers (SST, SSS, MLD, Chl *a* (before 1998 using a climatology), and atmospheric xCO_2) and gridded pCO_2 observations from SOCAT.

Main intention/focus: Produce global pCO_2 and CO_2 flux maps; investigate seasonal and inter-annual variability within the study period

Documentation: Landschützer et al. (2013, 2014).

Contact: Peter Landschützer.

A10 "*CARBONES-NN*"

Method description: CARBONES-NN is a neural network framework developed within the EU-FP7 project CARBONES (http://www.carbones.eu/wcmqs/) that maps surface ocean pCO_2 observations to first-order explanatory variables. As explanatory variables, it uses observations from satellites (Surface Chlorophyll climatology from SeaWiFS), model outputs (SST, SSS, MLD) from the MERCATOR ocean reanalysis, previous step pCO_2 estimates (recursive approach) and latitude as a proxy for atmospheric conditions. A two-step neural network approach is applied based on a Multi Layer Perceptron network coupled with a variational data assimilation scheme. A first calibration step adjusts the seasonal component of pCO_2 using climatological data (reference year 2000; from Takahashi et al., 2009 sampled at the points where there are measurements). This step recreates a 2-D monthly climatology of pCO_2 that is similar to the one of Takahashi et al. (2009), but also different as the interpolation is based on the explanatory variables. A second step uses the raw pCO_2 data (LDEOv1.0, Takahashi et al., 2007) to adjust the interannual variability of pCO_2 over the period 1989 to 2009. A moving assimilation window is used. Input variables and pCO_2 data were

BGD
12, 14049–14104, 2015

previously gridded at monthly temporal and 2° × 2° spatial resolutions. Note that most of the coastal ocean pCO_2 data have been filtered out.

Main intention/focus: Produce global CO_2 sea–air flux maps over the past decades to be coupled in the Carbon Cycle Data Assimilation System developed at LSCE within the CARBONES project.

Documentation: CARBONES web site (http://www.carbones.eu/wcmqs/) and article under preparation.

Contact: Philippe Peylin.

A11 "*NIES-SOM*"

Method description: Self-organizing map with linear increasing trend with time.

Main intention/focus: pCO_2 mapping and evaluating seasonal/interannual air–sea CO_2 exchange.

Documentation: Nakaoka et al. (2013) (for North Pacific); Nakaoka et al. (2015) (for Pacific).

Contact: Shin-ichiro Nakaoka.

A12 "*NIES-NN*" (feed-forward neural network)

Method description: We first estimated the global trend of pCO_2 using the method of Zeng et al. (2014) and used this trend to normalize the pCO_2 data to the reference year 2000. We then modelled the spatial and seasonal variations in the reference year using a feed-forward neural network (Zeng et al., 2015b). The driver variables include SST, SSS, Chl *a*, latitude, longitude, and month. For training, climatologies of the driver data are used. For prediction, we use time variant SST (it would be ideal to use time variant SSS and Chl *a* as well but no such data are available in certain modeled periods). Due to the use of climatologies of the driver data and the normalized pCO_2 to train the neural network, the predicted pCO_2 does not yet contain a trend; therefore, the trend estimated in the first step is re-added to the network output. We use all data from

BGD
12, 14049–14104, 2015

SOCATv2 that fulfill the selection criteria elevation < −500 m, ice cover < 50 %, SSS > 25, and SST > −10 °C. Software implementation details of the model can be found in Zeng et al. (2015a).

Main intention/focus: Monthly CO_2 maps and long-term global trend.

Documentation: Zeng et al. (2014) (for climatology); Zeng et al., 2015b (for time-varying fields); Zeng et al., 2015a (software implementation); data set doi:10.1594/PANGAEA.834398.

Contact: Jiye Zeng.

A13 "*PU-MCMC*"

Method description: The Princeton pCO_2 product is calculated by a Bayesian inversion (using a Markov Chain Monte Carlo (MCMC) minimization algorithm) as described in Majkut et al. (2014). The pCO_2 field is decomposed into (A) the decadal trend, (B) the June 1995 mean value, (C) the seasonal cycle, and (D) the interannual variability. Each of these terms is derived from process model simulations, and then scaled as to optimally fit the pCO_2 observations. The data product that is inverted is LDEOv2010 (Takahashi et al., 2012). Two forward models were used to derive the prior fields, with the main model being GFDL's MOM4p1-BLING. For MOM4p1-BLING the underlying physical model is GFDL's Modular Ocean Model version 4.1 (Griffies et al., 2004) with three degree horizontal resolution. The biogeochemical model is Biology Light Nutrient and Gas (BLING) (Galbraith et al., 2011). The model was forced at the surface with several reanalysis products, including CORE-II (Large and Yeager, 2009), ERA-40 (Uppala et al., 2005), and NCEP-1 (Kalnay et al., 1996). Additionally, the two simulations with NEMO-PISCES from the study of Rodgers et al. (2014) were included in the analysis.

Main intention/focus: Seasonal through decadal variability in pCO_2 and air–sea CO_2 fluxes.

Documentation: Majkut et al. (2014).

Contact: Keith Rodgers.

BGD
12, 14049–14104, 2015

A14 "*NIES-OTTM*" (Ocean Tracer Transport Model with variational assimilation of surface ocean pCO_2)

Method description: The offline OTTM is run with physical data from GFDL coupled ocean-atmospheric re-analysis version-2 data for the period of 1980–2010 (Delworth et al., 2006; Gnanadesikan et al., 2006). The necessary input data used from the re-analysis are as follows: The time dependent 3-D currents, hydrography and surface 2-D variables such as MLD, heat fluxes, water fluxes and sea surface height. The physical part of OTTM calculates the evolution of tracers in the global ocean (Valsala et al., 2008). The biological model is adapted from McKinley et al. (2004). The export production in the surface euphotic zone (0–140 m) is calculated using prescribed monthly climatological phosphate and light, scaled by a spatially varying "α" parameter which accounts for maximum export rate and for those processes which are not accounted for by the phosphate and light limitation model. The surface ocean chemistry model is taken from OCMIP-II abiotic model (Orr et al., 1999). The physical-biogeochemical model is used to simulate the surface ocean pCO_2 and air–sea CO_2 fluxes. The surface ocean pCO_2 in the model is constrained by a variational assimilation method in which a conservative adjoint of data-model misfit of pCO_2 (using the pCO_2 climatology and LDEOv1.0 point data, Takahashi et al., 2007) is tracked backward in time in the 3-D ocean over an iteration window of 2 months. At each iteration, the forward model corrects the initial and boundary condition of DIC (Dissolved Inorganic Carbon) according to the weighted adjoints. The iterations are truncated when the mismatch falls below a minimum value of 10 % of its initial value (see Valsala and Maksyutov, 2010).

Documentation: Valsala and Maksyutov (2010).

Contact: Vinu Valsala.

Acknowledgements. We would like to thank all colleagues and funding agencies involved in the collection, quality control, and synthetization of pCO_2 data, which are the basis of all mapping products. The Surface Ocean CO_2 Atlas (SOCAT) is an international effort, supported by the International Ocean Carbon Coordination Project (IOCCP), the Surface Ocean Lower Atmosphere Study (SOLAS), and the Integrated Marine Biogeochemistry and

BGD
12, 14049–14104, 2015

Ecosystem Research program (IMBER), to deliver a uniformly quality-controlled surface ocean CO_2 database. We cordially thank SOLAS (in particular Emilie Brevière) for kindly supporting the SOCOM kick-off meeting in Beijing (June 2013), and NIES (in particular Shin-ichiro Nakaoka and Yukihiro Nojiri) for kindly organizing and supporting the SOCOM progress meeting in Tsukuba (February 2015). We thank Amanda Fay for advise in using the biome map, and Martin Heimann for helpful comments on the manuscript. N. Metzl, N. Gruber, and P. Landschützer thank the EU FP7 project CARBOCHANGE (264879) for their support. N. Gruber and P. Landschützer also acknowledge funding from the EU FP7 project GEOCARBON (283080). J. D. Shutler gratefully acknowledges support by the European Space Agency project contract No. 4000112091/14/I-LG, and thanks Peter Land for his help in data preparation. A. R. Jacobson and K. B. Rodgers have been kindly supported by NASA grant NNX14AL85G.

The article processing charges for this open-access publication were covered by the Max Planck Society.

References

Bakker, D. C. E., Pfeil, B., Smith, K., Hankin, S., Olsen, A., Alin, S. R., Cosca, C., Harasawa, S., Kozyr, A., Nojiri, Y., O'Brien, K. M., Schuster, U., Telszewski, M., Tilbrook, B., Wada, C., Akl, J., Barbero, L., Bates, N. R., Boutin, J., Bozec, Y., Cai, W.-J., Castle, R. D., Chavez, F. P., Chen, L., Chierici, M., Currie, K., de Baar, H. J. W., Evans, W., Feely, R. A., Fransson, A., Gao, Z., Hales, B., Hardman-Mountford, N. J., Hoppema, M., Huang, W.-J., Hunt, C. W., Huss, B., Ichikawa, T., Johannessen, T., Jones, E. M., Jones, S. D., Jutterström, S., Kitidis, V., Körtzinger, A., Landschützer, P., Lauvset, S. K., Lefèvre, N., Manke, A. B., Mathis, J. T., Merlivat, L., Metzl, N., Murata, A., Newberger, T., Omar, A. M., Ono, T., Park, G.-H., Paterson, K., Pierrot, D., Ríos, A. F., Sabine, C. L., Saito, S., Salisbury, J., Sarma, V. V. S. S., Schlitzer, R., Sieger, R., Skjelvan, I., Steinhoff, T., Sullivan, K. F., Sun, H., Sutton, A. J., Suzuki, T., Sweeney, C., Takahashi, T., Tjiputra, J., Tsurushima, N., van Heuven, S. M. A. C., Vandemark, D., Vlahos, P., Wallace, D. W. R., Wanninkhof, R., and Watson, A. J.: An update to the Surface Ocean CO_2 Atlas (SOCAT version 2), Earth Syst. Sci. Data, 6, 69–90, doi:10.5194/essd-6-69-2014, 2014. 14052, 14059

Cressman, G. P.: An operational objective analysis system, Mon. Weather Rev., 87, 367–374, 1959. 14070

Delworth, T. L., Broccoli, A. J., Rosati, A., Stouffer, R. J., Balaji, V., Beesley, J. A., Cooke, W. F., Dixon, K. W., Dunne, J., Dunne, K. A., Durachta, J. W., Findell, K. L., Ginoux, P., Gnanadesikan, A., Gordon, C. T., Griffies, S. M., Gudgel, R., Harrison, M. J., Held, I. M., Hemler, R. S., Horowitz, L. W., Klein, S. A., Knutson, T. R., Kushner, P. J., Langenhorst, A. R., Lee, H.-C., Lin, S.-J., Lu, J., Malyshev, S. L., Milly, P. C. D., Ramaswamy, V., Russell, J., Schwarzkopf, M. D., Shevliakova, E., Sirutis, J. J., Spelman, M. J., Stern, W. F., Winton, M., Wittenberg, A. T., Wyman, B., Zeng, F., and Zhang, R.: GFDL's CM2 Global coupled climate models. Part I: Formulation and simulation characteristics, J. Clim., 19, 643–674, 2006. 14079

Fay, A. R. and McKinley, G. A.: Global open-ocean biomes: mean and temporal variability, Earth Syst. Sci. Data, 6, 273–284, doi:10.5194/essd-6-273-2014, 2014. 14058, 14068, 14093, 14095, 14096, 14097, 14099, 14100, 14102

Feely, R. A., Wanninkhof, R., Takahashi, T., and Tans, P.: Influence of El Niño on the equatorial Pacific contribution to atmospheric CO_2 accumulation, Nature, 398, 597–601, 1999. 14063

Galbraith, E., Kwon, E. Y., Gnanadesikan, A., Rodgers, K. B., Griffies, S. M., Bianchi, D., Sarmiento, J. L., Dunne, J. P., Simeon, J., Slater, R. D., Wittenberg, A. T., and Held, I. M.: Climate variability and radiocarbon in the CM2Mc Earth system model, J. Clim., 21, 4749–4765, 2011. 14078

Gloor, M., Gruber, N., Sarmiento, J., Sabine, C. L., Feely, R. A., and Rödenbeck, C.: A first estimate of present and preindustrial air–sea CO_2 flux patterns based on ocean interior carbon measurements and models, Geophys. Res. Lett., 30, 1010, doi:10.1029/2002GL015594, 2003. 14052

Gnanadesikan, A., Dixon, K., Griffies, S., Balaji, V., Barreiro, M., and co authors: GFDL's CM2 global coupled climate models. Part II: The baseline ocean simulation, J. Climate, 19, 675–697, 2006. 14079

Goddijn-Murphy, L. M., Woolf, D. K., Land, P. E., Shutler, J. D., and Donlon, C.: The OceanFlux Greenhouse Gases methodology for deriving a sea surface climatology of CO_2 fugacity in support of air–sea gas flux studies, Ocean Sci., 11, 519–541, doi:10.5194/os-11-519-2015, 2015. 14071

Griffies, S. M., Harrison, M. J., Pacanowski, R. C., Rosati, A.: A technical guide to MOM4, Tech. Rep., NOAA GFDL, Princeton, NJ, 2004. 14078

BGD
12, 14049–14104, 2015

Gruber, N., Gloor, M., Fletcher, S. E. M., Doney, S. C., Dutkiewicz, S., Follows, M. J., Gerber, M., Jacobson, A. R., Joos, F., Lindsay, K., Menemenlis, D., Mouchet, A., Müller, S. A., Sarmiento, J. L., and Takahashi, T.: Oceanic sources, sinks, and transport of atmospheric CO_2, Global Biogeochem. Cy., 23, GB1005, doi:10.1029/2008GB003349, 2009. 14068

Iida, Y., Kojima, A., Takatani, Y., Nakano, T., Midorikawa, T., and Ishii, M.: Trends in pCO_2 and sea–air CO_2 flux over the global open oceans for the last two decades., J. Oceanogr., doi:10.1007/s10872-015-0306-4, 2015. 14075, 14089

Jacobson, A. R., Mikaloff Fletcher, S. E., Gruber, N., Sarmiento, J. L., and Gloor, M.: A joint atmosphere–ocean inversion for surface fluxes of carbon dioxide: 1. Methods and global-scale fluxes, Global Biogeochem. Cy., 21, GB1019, doi:10.1029/2005GB002556, 2007. 14068

Jacobson, A. et al.: Trends in surface ocean pCO_2, Global Biogeochem. Cy., in preparation, 2015. 14072, 14073, 14089

Jones, S. D., Le Quéré, C., and Rödenbeck, C.: Autocorrelation characteristics of surface ocean pCO_2 and air–sea CO_2 fluxes, Global Biogeochem. Cy., 26, GB2042, doi:10.1029/2010GB004017, 2012. 14066, 14070

Jones, S. D., Le Quéré, C., Rödenbeck, C., and Manning, A.: A global interpolation of surface ocean pCO_2, J. Adv.n Model. Earth Sys., in revision, 2015. 14066, 14070, 14089

Kalnay, E., Kanamitsu, M., Kistler, R., Collins, W., Deaven, D., Gandin, L., Iredell, M., Saha, S., White, G., Woollen, J., Zhu, Y., Chelliah, M., Ebisuzaki, W., Higgins, W., Janowiak, J., Mo, K. C., Ropelewski, C., Wang, J., Leetmaa, A., Reynolds, R., Jenne, R., and Joseph, D.: The NCEP/NCAR 40-year reanalysis project, B. Am. Meteorol. Soc., 77, 437–471, 1996. 14061, 14078

Khatiwala, S., Tanhua, T., Mikaloff Fletcher, S., Gerber, M., Doney, S. C., Graven, H. D., Gruber, N., McKinley, G. A., Murata, A., Ríos, A. F., and Sabine, C. L.: Global ocean storage of anthropogenic carbon, Biogeosciences, 10, 2169–2191, doi:10.5194/bg-10-2169-2013, 2013. 14051

Kurihara, Y., Sakurai, T., and Kuragano, T.: Global daily sea surface temperature analysis using data from satellite microwave radiometer, satellite infrared radiometer and in-situ observations, Sokko-jiho, 73 S1–S18 , 2006 (in Japanese). 14074

Landschützer, P., Gruber, N., Bakker, D. C. E., Schuster, U., Nakaoka, S., Payne, M. R., Sasse, T. P., and Zeng, J.: A neural network-based estimate of the seasonal to inter-

BGD
12, 14049–14104, 2015

annual variability of the Atlantic Ocean carbon sink, Biogeosciences, 10, 7793–7815, doi:10.5194/bg-10-7793-2013, 2013. 14076

Landschützer, P., Gruber, N., Bakker, D. C. E., and Schuster, U.: Recent variability of the global ocean carbon sink, Global Biogeochem. Cy., 28, 927–949, 2014. 14076, 14089

Large, W. and Yeager, S.: The global climatology of an interannually varying air–sea flux data set, Clim. Dynam., 33, 341–364, 2009. 14078

Le Quéré, C., Moriarty, R., Andrew, R. M., Peters, G. P., Ciais, P., Friedlingstein, P., Jones, S. D., Sitch, S., Tans, P., Arneth, A., Boden, T. A., Bopp, L., Bozec, Y., Canadell, J. G., Chini, L. P., Chevallier, F., Cosca, C. E., Harris, I., Hoppema, M., Houghton, R. A., House, J. I., Jain, A. K., Johannessen, T., Kato, E., Keeling, R. F., Kitidis, V., Klein Goldewijk, K., Koven, C., Landa, C. S., Landschützer, P., Lenton, A., Lima, I. D., Marland, G., Mathis, J. T., Metzl, N., Nojiri, Y., Olsen, A., Ono, T., Peng, S., Peters, W., Pfeil, B., Poulter, B., Raupach, M. R., Regnier, P., Rödenbeck, C., Saito, S., Salisbury, J. E., Schuster, U., Schwinger, J., Séférian, R., Segschneider, J., Steinhoff, T., Stocker, B. D., Sutton, A. J., Takahashi, T., Tilbrook, B., van der Werf, G. R., Viovy, N., Wang, Y.-P., Wanninkhof, R., Wiltshire, A., and Zeng, N.: Global carbon budget 2014, Earth Syst. Sci. Data, 7, 47–85, doi:10.5194/essd-7-47-2015, 2015. 14051, 14054, 14066, 14067, 14069, 14073

Levitus, S.: Climatological Atlas of the World Ocean, United States Government Printing, Rockville, Md., 1982. 14070

Majkut, J. D., Sarmiento, J. L., and Rodgers, K. B.: A growing oceanic carbon uptake: Results from an inversion study of surface pCO_2 data, Global Biogeochem. Cy., 28, 335–351, 2014. 14078, 14089

Manning, A. C. and Keeling, R. F.: Global oceanic and land biotic carbon sinks from the Scripps atmospheric oxygen flask sampling network, Tellus B, 58, 95–116, 2006. 14068

Masarie, K. A. and Tans, P. P.: Extension and integration of atmospheric carbon dioxide data into a globally consistent measurement record, J. Geophys. Res., 100, 11593–11610, 1995. 14070

McKinley, G. A., Follows, M. J., and Marshall, J.: Mechanism of air–sea CO_2 flux variability in the equatorial Pacific and North Atlantic, Global Biogeochem. Cy., 18, GB2011, doi:10.1029/2003GB002179, 2004. 14079

Nakaoka, S., Telszewski, M., Nojiri, Y., Yasunaka, S., Miyazaki, C., Mukai, H., and Usui, N.: Estimating temporal and spatial variation of ocean surface pCO_2 in the North Pacific using a self-

BGD
12, 14049–14104, 2015

organizing map neural network technique, Biogeosciences, 10, 6093–6106, doi:10.5194/bg-10-6093-2013, 2013. 14077, 14089

Orr, J. C., Najjar, R., Sabine, C. L., and Joos, F.: Abiotic-HOWTO, LSCE/CEA Saclay, Gif-sur-Yvette, France, 25 pp., 1999. 14079

Park, G.-H., Wanninkhof, R., Doney, S. C., Takahashi, T., Lee, K., Feely, R. A., Sabine, C. L., Triñanes, J., and Lima, I. D.: Variability of global net sea–air CO_2 fluxes over the last three decades using empirical relationships, Tellus B, 62, 352–368, 2010a. 14073, 14089

Park, G.-H., Wanninkhof, R., and Trinanes, J.: Procedures to create near real-time seasonal air–sea CO_2 flux maps, Atlantic Oceanographic and Meteorological Laboratory, NOAA Technical Memorandum-98, OAR AOML, Miami, 2010b. 14073

Peylin, P., Law, R. M., Gurney, K. R., Chevallier, F., Jacobson, A. R., Maki, T., Niwa, Y., Patra, P. K., Peters, W., Rayner, P. J., Rödenbeck, C., van der Laan-Luijkx, I. T., and Zhang, X.: Global atmospheric carbon budget: results from an ensemble of atmospheric CO_2 inversions, Biogeosciences, 10, 6699–6720, doi:10.5194/bg-10-6699-2013, 2013. 14052, 14067

Rödenbeck, C.: Estimating CO_2 sources and sinks from atmospheric mixing ratio measurements using a global inversion of atmospheric transport, Tech. Rep. 6, Max Planck Institute for Biogeochemistry, Jena, Germany, 2005. 14072

Rödenbeck, C., Keeling, R. F., Bakker, D. C. E., Metzl, N., Olsen, A., Sabine, C., and Heimann, M.: Global surface-ocean p^{CO_2} and sea–air CO_2 flux variability from an observation-driven ocean mixed-layer scheme, Ocean Sci., 9, 193–216, doi:10.5194/os-9-193-2013, 2013. 14058, 14061, 14072

Rödenbeck, C., Bakker, D. C. E., Metzl, N., Olsen, A., Sabine, C., Cassar, N., Reum, F., Keeling, R. F., and Heimann, M.: Interannual sea–air CO_2 flux variability from an observation-driven ocean mixed-layer scheme, Biogeosciences, 11, 4599–4613, doi:10.5194/bg-11-4599-2014, 2014. 14067, 14072, 14089

Rodgers, K. B., Aumont, O., Mikaloff Fletcher, S. E., Plancherel, Y., Bopp, L., de Boyer Montégut, C., Iudicone, D., Keeling, R. F., Madec, G., and Wanninkhof, R.: Strong sensitivity of Southern Ocean carbon uptake and nutrient cycling to wind stirring, Biogeosciences, 11, 4077–4098, doi:10.5194/bg-11-4077-2014, 2014. 14078

Sabine, C. L., Feely, R. A., Gruber, N., Key, R. M., Lee, K., Bullister, J. L., Wanninkhof, R., Wong, C. S., Wallace, D. W. R., Tilbrook, B., Millero, F. J., Peng, T.-H., Kozyr, A., Ono, T., and Rios, A.: The oceanic sink for anthropogenic CO_2, Science, 305, 367–371, 2004. 14051

BGD
12, 14049–14104, 2015

Sabine, C. L., Hankin, S., Koyuk, H., Bakker, D. C. E., Pfeil, B., Olsen, A., Metzl, N., Kozyr, A., Fassbender, A., Manke, A., Malczyk, J., Akl, J., Alin, S. R., Bellerby, R. G. J., Borges, A., Boutin, J., Brown, P. J., Cai, W.-J., Chavez, F. P., Chen, A., Cosca, C., Feely, R. A., González-Dávila, M., Goyet, C., Hardman-Mountford, N., Heinze, C., Hoppema, M., Hunt, C. W., Hydes, D., Ishii, M., Johannessen, T., Key, R. M., Körtzinger, A., Landschützer, P., Lauvset, S. K., Lefèvre, N., Lenton, A., Lourantou, A., Merlivat, L., Midorikawa, T., Mintrop, L., Miyazaki, C., Murata, A., Nakadate, A., Nakano, Y., Nakaoka, S., Nojiri, Y., Omar, A. M., Padin, X. A., Park, G.-H., Paterson, K., Perez, F. F., Pierrot, D., Poisson, A., Ríos, A. F., Salisbury, J., Santana-Casiano, J. M., Sarma, V. V. S. S., Schlitzer, R., Schneider, B., Schuster, U., Sieger, R., Skjelvan, I., Steinhoff, T., Suzuki, T., Takahashi, T., Tedesco, K., Telszewski, M., Thomas, H., Tilbrook, B., Vandemark, D., Veness, T., Watson, A. J., Weiss, R., Wong, C. S., and Yoshikawa-Inoue, H.: Surface Ocean CO_2 Atlas (SOCAT) gridded data products, Earth Syst. Sci. Data, 5, 145–153, doi:10.5194/essd-5-145-2013, 2013. 14059, 14074

Sasse, T. P., McNeil, B. I., and Abramowitz, G.: A new constraint on global air–sea CO_2 fluxes using bottle carbon data, Geophys. Res. Lett., 40, 1594–1599, 2013. 14075, 14089

Schuster, U., Watson, A. J., Bates, N. R., Corbière, A., González-Dávila, M., Metzl, N., Pierrot, D., and Santana-Casiano, J. M.: Trends in North Atlantic sea-surface fCO_2 from 1990 to 2006, Deep-Sea Res. Pt. II, 56, 620–629, 2009. 14070

Schuster, U., McKinley, G. A., Bates, N., Chevallier, F., Doney, S. C., Fay, A. R., González-Dávila, M., Gruber, N., Jones, S., Krijnen, J., Landschützer, P., Lefèvre, N., Manizza, M., Mathis, J., Metzl, N., Olsen, A., Rios, A. F., Rödenbeck, C., Santana-Casiano, J. M., Takahashi, T., Wanninkhof, R., and Watson, A. J.: An assessment of the Atlantic and Arctic sea–air CO_2 fluxes, 1990–2009, Biogeosciences, 10, 607–627, doi:10.5194/bg-10-607-2013, 2013. 14062, 14063, 14074, 14089

Séférian, R., Ribes, A., and Bopp, L.: Detecting the anthropogenic influences on recent changes in ocean carbon uptake, Geophys. Res. Lett., 41, 5968–5977, doi:10.1002/2014GL061223, 2014. 14067

Shutler, J. D., Land, P. E., Piolle, J.-F., Woolf, D. K., Goddijn-Murphy, L., Paul, F., Girard-Ardhuin, F., Chapron, B., and Donlon, C.: FluxEngine: A flexible processing system for calculating atmosphere–ocean carbon dioxide gas fluxes and climatologies, J. Atmos. Ocean. Tech., in revision, 2015. 14071, 14089

Stocker, T., Qin, D., Plattner, G.-K., Tignor, M., Allen, S., Boschung, J., Nauels, A., Xia, Y., Bex, V., and Midgley, P. (Eds.): Climate Change 2013: The Physical Science Basis. Contri-

bution of Working Group I to the Fifth Assessment Report of the Intergovernmental Panel on Climate Change, Cambridge University Press, Cambridge, UK and New York, NY, USA, 2013. 14051

Takahashi, T., Sutherland, S., and Kozyr, A.: Global Ocean Surface Water Partial Pressure of CO_2 Database: Measurements Performed During 1968-2006 (Version 1.0), ORNL/CDIAC-152, NDP-088, Carbon Dioxide Information Analysis Center, Oak Ridge National Laboratory, U. S. Department of Energy, Oak Ridge, Tennessee, 20 pp., 2007. 14076, 14079

Takahashi, T., Sutherland, S. C., Wanninkhof, R., Sweeney, C., Feely, R. A., Chipman, D. W., Hales, B., Friederich, G., Chavez, F., Sabine, C., Watson, A., Bakker, D. C. E., Schuster, U., Metzl, N., Yoshikawa-Inoue, H., Ishii, M., Midorikawa, T., Nojiri, Y., Kortzinger, A., Steinhoff, T., Hoppema, M., Olafsson, J., Arnarson, T. S., Tillbrook, B., Johannessen, T., and Olsen, A., Bellerby, R., Wong, C. S., Delille, B., Bates, N. R., and de Baar, H. J. W.: Climatological mean and decadal change in surface ocean pCO_2 and net sea–air CO_2 flux over the global oceans, Deep-Sea Res. Pt. II, 56, 554–577, 2009. 14061, 14072, 14076

Takahashi, T., Sutherland, S., and Kozyr, A.: Global ocean surface water partial pressure of CO_2 database, Measurements performed during 1957–2011 (version 2011), ORNL/CDIAC-160, NDP-088(V2011), Carbon Dioxide Information Analysis Center, Oak Ridget National Laboratory, U. S. Department of Energy, Oak Ridge, Tennessee, 2012. 14078

Takahashi, T., Sutherland, S., and Kozyr, A.: Global Ocean Surface Water Partial Pressure of CO_2 Database: Measurements Performed During 1957-2013 (Version 2013), ORNL/CDIAC-160, NDP-088(V2013), Carbon Dioxide Information Analysis Center, Oak Ridge National Laboratory, U. S. Department of Energy, Oak Ridge, Tennessee, 2014a. 14052, 14060

Takahashi, T., Sutherland, S. C., Chipman, D. W., Goddard, J. G., Newberger, T., and Sweeney, C.: Climatological Distributions of pH, pCO_2, Total CO_2, Alkalinity, and $CaCO_3$ Saturation in the Global Surface Ocean, ORNL/CDIAC-160, NDP-094. Carbon Dioxide Information Analysis Center, Oak Ridge National Laboratory, U. S. Department of Energy, Oak Ridge, Tennessee, doi:10.3334/CDIAC/OTG.NDP094, 2014b. 14058

Telszewski, M., Chazottes, A., Schuster, U., Watson, A. J., Moulin, C., Bakker, D. C. E., González-Dávila, M., Johannessen, T., Körtzinger, A., Lüger, H., Olsen, A., Omar, A., Padin, X. A., Ríos, A. F., Steinhoff, T., Santana-Casiano, M., Wallace, D. W. R., and Wanninkhof, R.: Estimating the monthly pCO_2 distribution in the North Atlantic using a self-organizing neural network, Biogeosciences, 6, 1405–1421, doi:10.5194/bg-6-1405-2009, 2009. 14056

BGD
12, 14049–14104, 2015

Turi, G., Lachkar, Z., and Gruber, N.: Spatiotemporal variability and drivers of pCO_2 and air–sea CO_2 fluxes in the California Current System: an eddy-resolving modeling study, Biogeosciences, 11, 671–690, doi:10.5194/bg-11-671-2014, 2014. 14067

Uppala, S. M., Kållberg, P. W., Simmons, A. J., Andrae, U., Bechtold, V. D. C., Fiorino, M., Gibson, J. K., Haseler, J., Hernandez, A., Kelly, G. A., Li, X., Onogi, K., Saarinen, S., Sokka, N., Allan, R. P., Andersson, E., Arpe, K., Balmaseda, M. A., Beljaars, A. C. M., Berg, L. V. D., Bidlot, J., Bormann, N., Caires, S., Chevallier, F., Dethof, A., Dragosavac, M., Fisher, M., Fuentes, M., Hagemann, S., Hólm, E., Hoskins, B. J., Isaksen, L., Janssen, P. A. E. M., Jenne, R., Mcnally, A. P., Mahfouf, J.-F., Morcrette, J.-J., Rayner, N. A., Saunders, R. W., Simon, P., Sterl, A., Trenberth, K. E., Untch, A., Vasiljevic, D., Viterbo, P., , and Woollen, J.: The ERA-40 re-analysis, Q. J. R. Meteorolog. Soc., 131, 2961–3012, 2005. 14078

U. S. Department Commerce: 2-minute gridded global relief data (ETOPO2v2), Natl. Oceanic and Atmos. Admin., Natl. Geophys. Data Cent, available at: http://www.ngdc.noaa.gov/mgg/fliers/06mgg01.html (last access: 2 March 2011), 2006. 14057

Usui, N., Ishizaki, S., Fujii, Y., Tsujino, H., Yasuda, T., and Kamachi, M.: Meteorological research institute multivariate ocean variational estimation (MOVE) system: some early results., Adv. Space Res., 37, 806–822, 2006. 14074

Valsala, K. V. and Maksyutov, S.: Simulation and assimilation of global ocean pCO_2 and air–sea CO_2 fluxes using ship observations of surface ocean pCO_2 in a simplified Biogeochemical offline model, Tellus B, 62, 821–840, 2010. 14063, 14079, 14089

Valsala, K. V., Maksyutov, S., and Ikeda, M.: Design and validation of an offline oceanic tracer transport model for a carbon cycle study, J. Climate, 21, 2752–2769, 2008. 14079

Wanninkhof, R.: Relationship between wind speed and gas exchange over the ocean, J. Geophys. Res.-Oceans, 97, 7373–7382, 1992. 14061

Wanninkhof, R., Park, G.-H., Takahashi, T., Sweeney, C., Feely, R., Nojiri, Y., Gruber, N., Doney, S. C., McKinley, G. A., Lenton, A., Le Quéré, C., Heinze, C., Schwinger, J., Graven, H., and Khatiwala, S.: Global ocean carbon uptake: magnitude, variability and trends, Biogeosciences, 10, 1983–2000, doi:10.5194/bg-10-1983-2013, 2013. 14052

Yu, L. and Weller, R. A.: Objectively Analyzed air–sea heat Fluxes (OAFlux) for the global oceans, B. Am. Meteorol. Soc., 88, 527–539, 2007. 14061

Zeng, J., Nojiri, Y., Landschützer, P., Telszewski, M., and Nakaoka, S.: A global surface ocean fCO_2 climatology based on a feed-forward neural network, J. Atmos. Ocean. Tech., 31, 1838–1849, 2014. 14077, 14078, 14089

Zeng, J., Nakajima, H., Nojiri, Y., and Nakaoka, S.: Reconstructing the Carbon Dioxide Absorption Patterns of World Oceans Using a Feed-Forward Neural Network: Software Implementation and Employment Techniques, 417–425, 2015a. 14078

Zeng, J. and Nojiri, Y. and Nakaoka, S. and Nakajima, H. and Shirai, T.: Surface ocean CO_2 in 1990–2011 modelled using a feed-forward neural network, Geosci. Data J., 2, 47–51, 2015. 14077, 14078

BGD

12, 14049–14104, 2015

An ensemble of pCO_2-based sea–air CO_2 flux estimates

C. Rödenbeck et al.

Table 1. General information on the mapping methods.

	Version used	Contact	Reference	Method type
UEA-SI	v1.0	Steve Jones	Jones et al. (2015)	Stat. Interpol.
OceanFlux-SI	v0.95	Jamie Shutler	Shutler et al. (2015)	Stat. Interpol.
Jena-MLS	oc_v1.2	Christian Rödenbeck	Rödenbeck et al. (2014)	Stat. Interpol.
CU-SCSE	v1.0	Andy Jacobson	Jacobson et al. (2015)	Stat. Interpol.
AOML-EMP	v2	Geun-Ha Park	Park et al. (2010a)	Regression
UEx-MLR	v2.0	Ute Schuster	Schuster et al. (2013)	Regression
JMA-MLR	v2	Yosuke Iida	Iida et al. (2015)	Regression
UNSW-SOMLO	v1	Tristan Sasse	Sasse et al. (2013)	Regression
ETH-SOMFFN	ETH30yr01	Peter Landschützer	Landschützer et al. (2014)	Regression
CARBONES-NN	18 February 2014	Philippe Peylin	http://www.carbones.eu/wcmqs/	Regression
NIES-SOM	v1.2	Shin-ichiro Nakaoka	update of Nakaoka et al. (2013)	Regression
NIES-NN	v1.0	Jiye Zeng	Zeng et al. (2014)	Regression
PU-MCMC	v1.0	Keith Rodgers	Majkut et al. (2014)	Model-based
NIES-OTTM	11 August 2013	Vinu Valsala	Valsala and Maksyutov (2010)	Model-based

BGD
12, 14049–14104, 2015

CC BY

Table 2. Original domains and grid resolutions of the products.

	Original domain –spatially[a]	–temporally	Original grid resolution –spatially	–temporally
UEA-SI	Global (up to 70° N)	1985–2011	2.5° × 2.5°	monthly
OceanFlux-SI	Global	1995–2009	1° × 1°	monthly
Jena-MLS	Global	1986–2011	≈ 4° × 5°	daily
CU-SCSE	Global	1970–2011	1° × 1°	monthly
AOML-EMP	Global	1985–2011	≈ 4° × 5°	monthly
UEx-MLR	Global	1990–2012	1° × 1°	monthly
JMA-MLR	Global	1990–2012 (Chl IAV since 1997)	1° × 1°	monthly
UNSW-SOMLO	Global (open-ocean)	1998–2011	1° × 1°	monthly
ETH-SOMFFN	Global (up to 79° N)	1982–2011	1° × 1°	monthly
CARBONES-NN	Global	1990–2009	2° × 2°	monthly
NIES-SOM	Global	1998–2009	1° × 1°	monthly
NIES-NN	Global	1990–2012	1° × 1°	monthly
PU-MCMC	Global	1980–2009	4° × 5°	monthly
NIES-OTTM	Global	1980–2010	1° × 1°	monthly

[a] Even if designated "global", most methods exclude some coastal areas or the Arctic, or treat coastal areas as open ocean.

BGD
12, 14049–14104, 2015

Table 3. Specifications of the mapping methods with respect to the constraints and assumptions used (see Appendix A for details and references)

	pCO_2 data	Adjusted variable	Coherence scales of adjustments[e] –spatially	–temporally	Regression of pCO_2 against	Prescribed relation
UEA-SI	SOCATv2	pCO_2	Correlated pixels	1–4 harmonics	–/–	–/–
OceanFlux-SI	SOCATv2	pCO_2	Correlated pixels	Correlated time steps	–/–	–/–
Jena-MLS	SOCATv2	Internal C fluxes[c]	Correlated pixels	Correlated days	–/–	–/–
CU-SCSE	SOCATv2	Pattern magnitudes	10 ocean basins	Correlated time steps[g]	Spatial basis functions (EOFs based on models)	Linear
AOML-EMP	Takah. clim.	Regr. coeff.	Independent pixels	1–4 sub-annual periods	SST	Linear
UEx-MLR	SOCATv2[a]	Regr. coeff.	20 ocean regions	Entire period	SST, MLD, Chl, pCO_2^{atm}	Linear
JMA-MLR	SOCATv2[b]	Regr. coeff.	44 regions	Entire period	SST, SSS, Chl	Linear
UNSW-SOMLO	SOCATv2	Regr. coeff.	Biogeochem. fingerprints[f]	Entire period	SST, SSS, MLD, Chl, xCO_2	Lin. (Non-lin.)[f]
ETH-SOMFFN	SOCATv2	Network weights	Biogeochem. provinces	Entire period	SST, SSS, MLD, Chl, xCO_2	Non-linear
CARBONES-NN	LDEOv1.0	Network weights	Global	Moving window	SST, SSS, MLD, Chl, lat[h], long[h]	Non-linear
NIES-SOM	SOCATv2	Assignments	Global	Entire period	SST, SSS, MLD, Chl, lat, long, time	Non-linear
NIES-NN	SOCATv2[a,b]	Network weights	Global	Entire period	SST, SSS, Chl, lat, long, month	Non-linear
PU-MCMC	LDEO2010	Regr. coeff.	Independent pixels	Entire period	Mean, trend, seas., and IAV from model simulation	Scaled model
NIES-OTTM	LDEOv1.0	IC + BC of DIC[d]	Independent pixels	2 months windows	Various drivers through the process model	Model

[a] Plus additional recent data
[b] Except some coastal data.
[c] Ocean-internal sources and sinks of carbon to the mixed layer.
[d] Initial and boundary conditions of the DIC field.
[e] Spatial and temporal domains of the adjustable degrees of freedom. Roughly speaking, pCO_2 structures *within* these domains originate from the structures in the driving variables, while structures *between* these domains are directly determined by the pCO_2 data. Thus, the coherence scales determine the balance between the ability of a method to bridge data gaps and its ability to directly follow the observed signals.
[f] The fingerprints are derived by non-linear clustering of the data themselves, thus the mapping as a whole is non-linear.
[g] The individual basis functions have widely different relaxation time scales (3 months – 5 years).
[h] Only for step 1 (seasonality), not for step 2 (IAV).
Glossary: Regr. coeff. = Regression coefficients, lat = latitude, long = longitude
Variables: Chl = Chlorophyll *a*, MLD = Mixed layer depth, SSS = Sea Surface Salinity, SST = Sea Surface Temperature, xCO_2 = Atmospheric CO_2 mixing ratio.

BGD
12, 14049–14104, 2015

CC BY

Table 4. Information content about various modes of variability as implemented by the individual mapping methods. Modes labelled as "EST." (= estimated) are considered to reflect data-based information, as they either are directly estimated by time-dependent adjustments, or are regressed against drivers through multiple adjustable degrees of freedom. The trend is considered estimated if the interannual degrees of freedom allow a data-based trend to establish or if pCO_2 is explicitly regressed against a rising term (time or atmospheric CO_2).

Method	Mean	Seasonality	IAV	Trend	Day-to-day
UEA-SI	EST.	EST.	partly est.	EST.	–/–
OceanFlux-SI	EST.	EST.	parameterized	prescribed	–/–
Jena-MLS	EST.	EST.	EST.	EST.	parameterized
CU-SCSE	EST.	EST.	EST.	EST.	interpolated
AOML-EMP	EST.	EST.	EST.	modelled	–/–
UEx-MLR	EST.	EST.	EST.	EST.	–/–
JMA-MLR	EST.	EST.	EST.	prescribed	–/–
UNSW-SOMLO	EST.	EST.	EST.	EST.	–/–
ETH-SOMFFN	EST.	EST.	EST.	EST.	–/–
CARBONES-NN	EST.	EST.	EST.	EST.	–/–
NIES-SOM	EST.	EST.	EST.	EST.	–/–
NIES-NN	EST.	EST.	EST.	EST.	–/–
PU-MCMC	EST.	scaled model	scaled model	EST.	–/–
NIES-OTTM	EST.	EST.	EST.	–/–	–/–

BGD
12, 14049–14104, 2015

CC BY

Table 5. Biomes of (Fay and McKinley, 2014) used for time series comparison (see Fig. 2).

No.	Abbreviation	Name
1	NP ICE	(omitted) North Pacific Ice
2	NP SPSS	North Pacific Subpolar Seasonally Stratified
3	NP STSS	North Pacific Subtropical Seasonally Stratified
4	NP STPS	North Pacific Subtropical Permanently Stratified
5	PEQU-W	West Pacific Equatorial
6	PEQU-E	East Pacific Equatorial
7	SP STPS	South Pacific Subtropical Permanently Stratified
8	NA ICE	(omitted) North Atlantic Ice
9	NA SPSS	North Atlantic Subpolar Seasonally Stratified
10	NA STSS	North Atlantic Subtropical Seasonally Stratified
11	NA STPS	North Atlantic Subtropical Permanently Stratified
12	AEQU	Atlantic Equatorial
13	SA STPS	South Atlantic Subtropical Permanently Stratified
14	IND STPS	Indian Ocean Subtropical Permanently Stratified
15	SO STSS	Southern Ocean Subtropical Seasonally Stratified
16	SO SPSS	Southern Ocean Subpolar Seasonally Stratified
17	SO ICE	Southern Ocean Ice

BGD
12, 14049–14104, 2015

CC BY

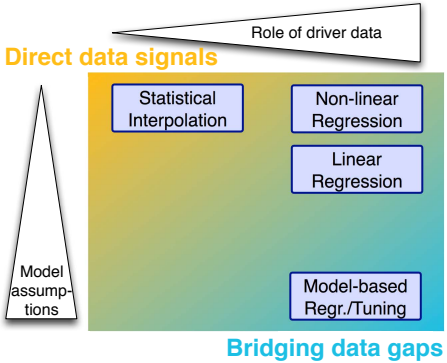

Figure 1. Classes of pCO_2 mapping methods: *Statistical interpolation methods* essentially only use the pCO_2 data themselves, filling spatio-temporal gaps by assuming a statistical relation to neighbouring data points. In well-constrained areas/periods, they closely follow the signals contained in the data, while in areas/periods far from neighbouring data points, they remain essentially unconstrained. *Regression methods* establish a quantitative relation between pCO_2 and a set of external variables assumed to capture the major modes of spatio-temporal variability. Adjustable degrees of freedom are constant in time and within certain spatial regions, such that data gaps can be filled according to the spatio-temporal structure in the external variables; however, variability not contained in any of the chosen external data sets cannot be reproduced. Non-linear regression methods (feed-forward neural networks, self-organizing maps) essentially do not impose any structure to this relation between pCO_2 and the drivers. (Multi-)linear regression imposes a linear relationship, thereby restricting the type of responses but ensuring a unique and mathematically well-defined solution. Finally, knowledge of biogeochemical processes can be brought to bear by regression of pCO_2 against fields simulated by a *biogeochemical process model*, or by tuning initial conditions or parameters in such a model simulation to match the observations. However, this relies heavily on the structure of the process simulation to be correct.

BGD
12, 14049–14104, 2015

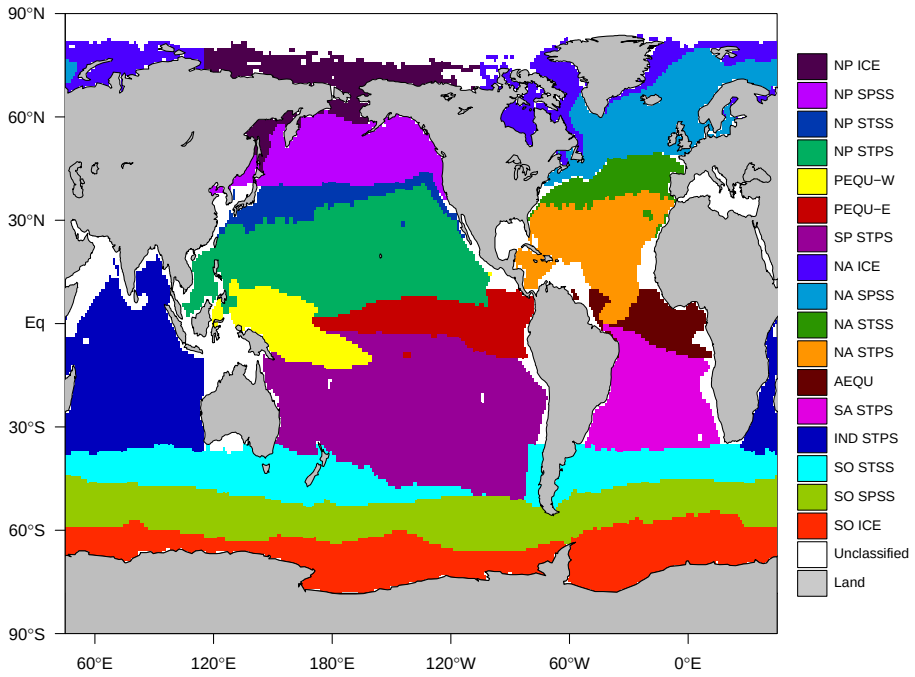

Figure 2. Map of biomes (Fay and McKinley, 2014) used for time series comparison. (See Table 5 for biome names.)

BGD
12, 14049–14104, 2015

An ensemble of pCO_2-based sea–air CO_2 flux estimates

C. Rödenbeck et al.

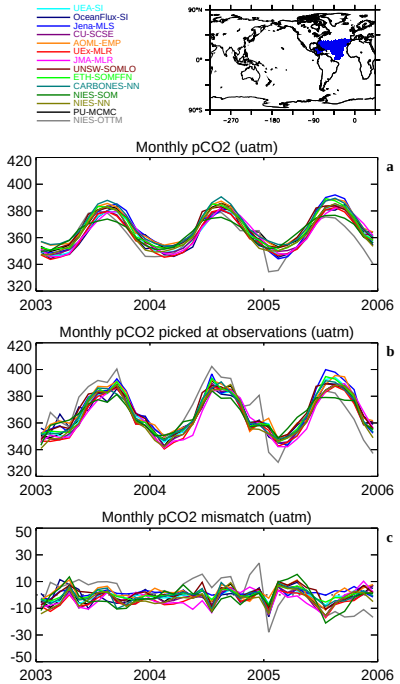

Figure 3. pCO_2 time series from the presented 14 mapping methods averaged over the North Atlantic Subtropical Permanently Stratified biome of Fay and McKinley (2014, illustrated by the little map on top). **(a)** pCO_2 on submitted monthly time steps for 3 selected years. **(b)** As **(a)**, but averages only calculated over pixels with actual data in the SOCATv2 monthly gridded data set. **(c)** Mismatch: biome-average difference between the submitted pCO_2 fields and the co-located SOCATv2 monthly gridded values.

BGD
12, 14049–14104, 2015

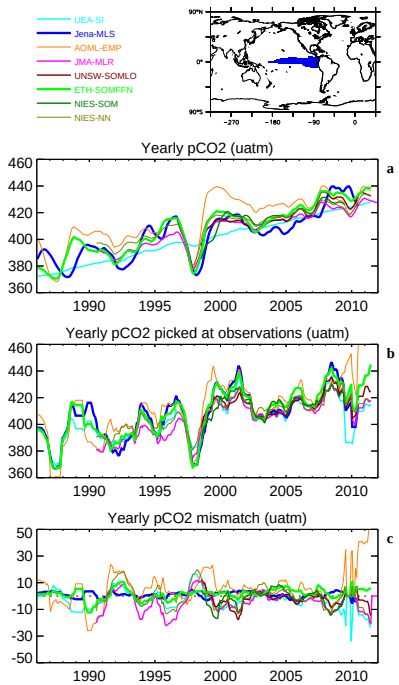

Figure 4. pCO_2 time series from selected mapping methods (having relative IAV mismatch $R^{iav} < 75\,\%$) averaged over the East Pacific Equatorial biome of Fay and McKinley (2014, illustrated by the little map on top). Line styles indicate the relative IAV mismatch: $R^{iav} < 30\,\%$ (thick), 30–60 % (medium), 60–75 % (thin). **(a)** Interannual pCO_2 variations (12 months running mean). **(b)** As **(a)**, but averages only calculated over pixels with actual data in the SOCATv2 monthly gridded data set. **(c)** Mismatch: biome/yearly-average difference between the submitted pCO_2 fields and the co-located SOCATv2 monthly gridded values.

BGD
12, 14049–14104, 2015

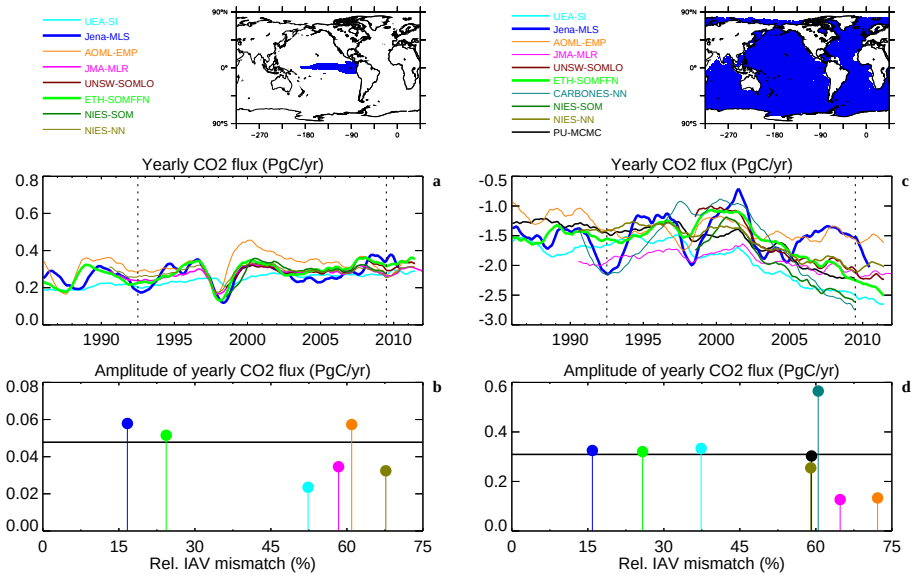

Figure 5. Interannual sea–air CO_2 flux variations in the East Pacific Equatorial biome (left) and the global ocean (right) from selected mapping methods (having relative IAV mismatch $R^{\mathrm{iav}} < 75\,\%$ for pCO_2 averaged in the respective region). **(a, c)** Time series (yearly flux sum). Line styles indicate the relative IAV mismatch: $R^{\mathrm{iav}} < 30\,\%$ (thick), 30–60 % (medium), 60–75 % (thin). The vertical dotted lines delimit the analysis period for the amplitude computation. **(b, d)** Amplitudes A_i^{iav} of interannual CO_2 flux variations (see Sect. 4.2) plotted against the relative IAV mismatch amplitude R_i^{iav} for each submission (cases not fully covering the analysis period have been omitted to avoid inconsistencies). The weighted mean $\overline{A^{\mathrm{iav}}}$ (Eq. 3) is given as horizontal line.

BGD
12, 14049–14104, 2015

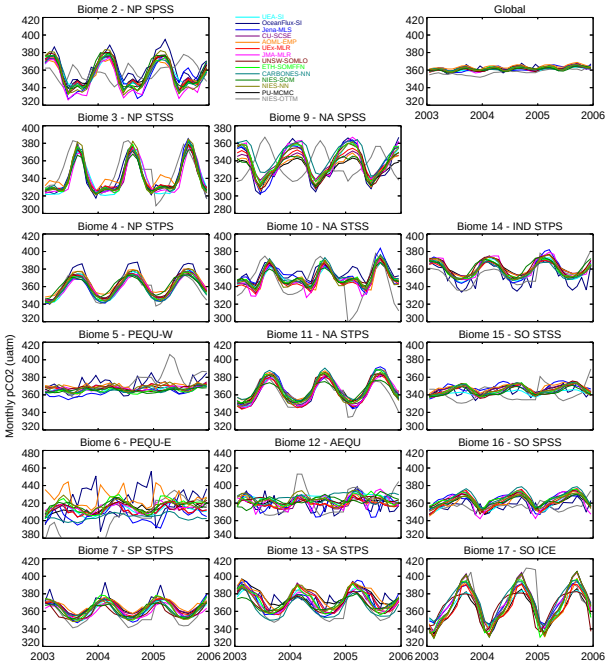

Figure A1. Monthly pCO_2 variations over 3 arbitrary years as estimated by all mapping methods, averaged over the biomes by Fay and McKinley (2014) (see Fig. 2, panels roughly in geographical arrangement). Vertical scales span the same range for all biomes (100 µatm), but some vertical shift has been chosen according to the mean spatial pCO_2 pattern. In some biomes, lines of certain mapping methods with higher mismatches have been clipped (rather than enlarging the vertical scale), in order to maintain clarity. Biomes 1 (North Pacific Ice) and 8 (North Atlantic Ice) have been omitted due to extremely sparse data coverage.

BGD
12, 14049–14104, 2015

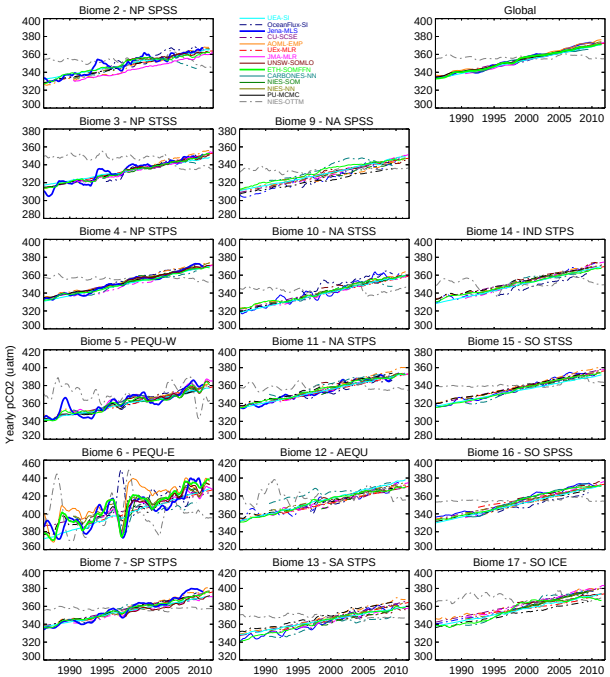

Figure A2. Interannual pCO_2 variations as estimated by all mapping methods, averaged over the biomes by Fay and McKinley (2014) (see Fig. 2, panels roughly in geographical arrangement). Line styles indicate the relative IAV mismatch: $R^{iav} < 30\,\%$ (thick), 30–60 % (medium), 60–75 % (thin), above 75 % (dashed); the legend reflects "Global". Vertical scales span the same range for all biomes (100 µatm), but some vertical shift has been chosen according to the mean spatial pCO_2 pattern. In some biomes, lines of certain mapping methods with higher mismatches have been clipped (rather than enlarging the vertical scale), in order to maintain clarity. Biomes 1 (North Pacific Ice) and 8 (North Atlantic Ice) have been omitted due to extremely sparse data coverage.

BGD
12, 14049–14104, 2015

CC BY

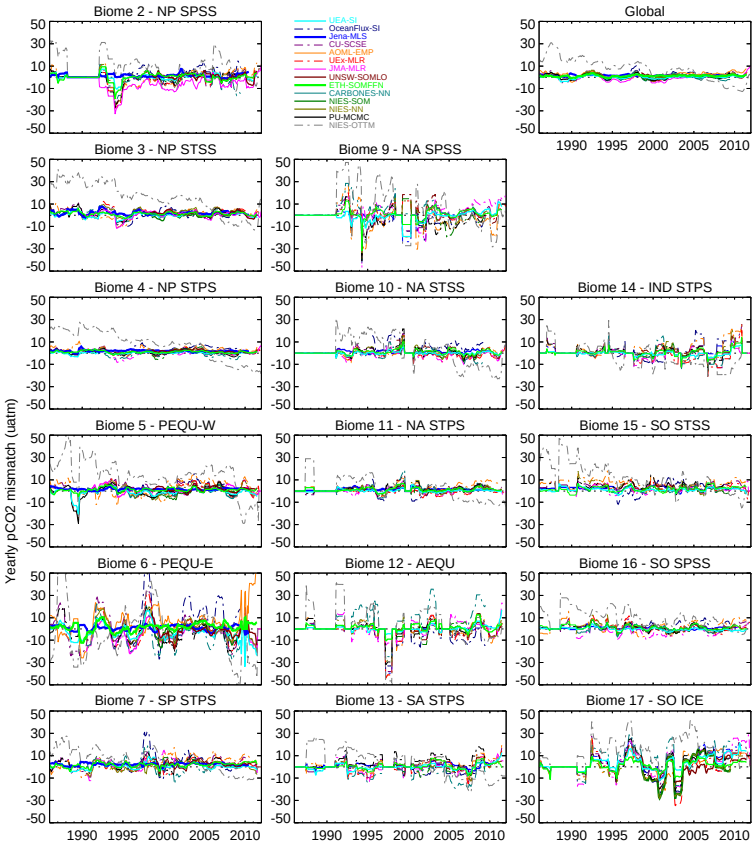

Figure A3. Mismatch between the interannual pCO_2 variations as estimated by all mapping methods and the SOCATv2 monthly gridded values.

BGD
12, 14049–14104, 2015

An ensemble of pCO_2-based sea–air CO_2 flux estimates

C. Rödenbeck et al.

CC BY

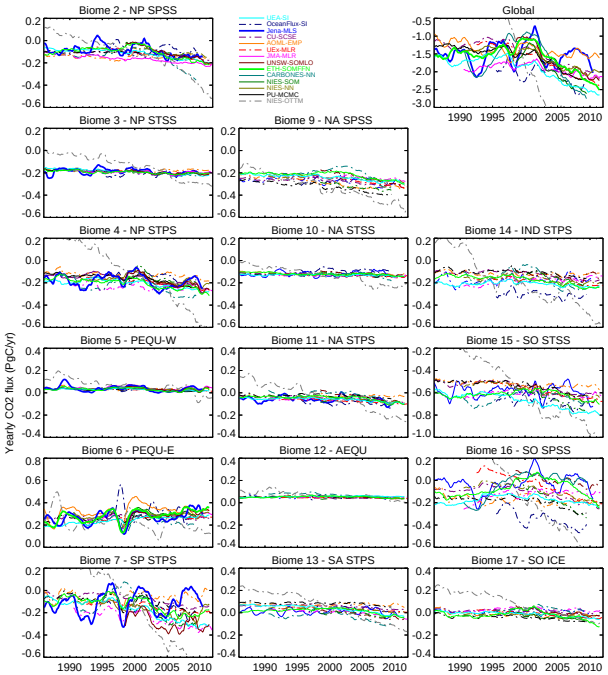

Figure A4. Interannual variations of the sea–air CO_2 flux as estimated by all mapping methods, integrated over the biomes by Fay and McKinley (2014) (see Fig. 2, panels roughly in geographical arrangement). Line styles indicate the relative IAV mismatch: $R^{\mathrm{iav}} < 30\,\%$ (thick), 30–60 % (medium), 60–75 % (thin), above 75 % (dashed); the legend reflects "Global". Vertical scales span the same range for all biomes (0.8 $\mathrm{PgC\,yr^{-1}}$ except the global flux), but some vertical shift has been chosen according to the mean spatial flux pattern. In some biomes, lines of certain mapping methods with higher mismatches have been clipped (rather than enlarging the vertical scale), in order to maintain clarity. Biomes 1 (North Pacific Ice) and 8 (North Atlantic Ice) have been omitted due to extremely sparse data coverage.

BGD
12, 14049–14104, 2015

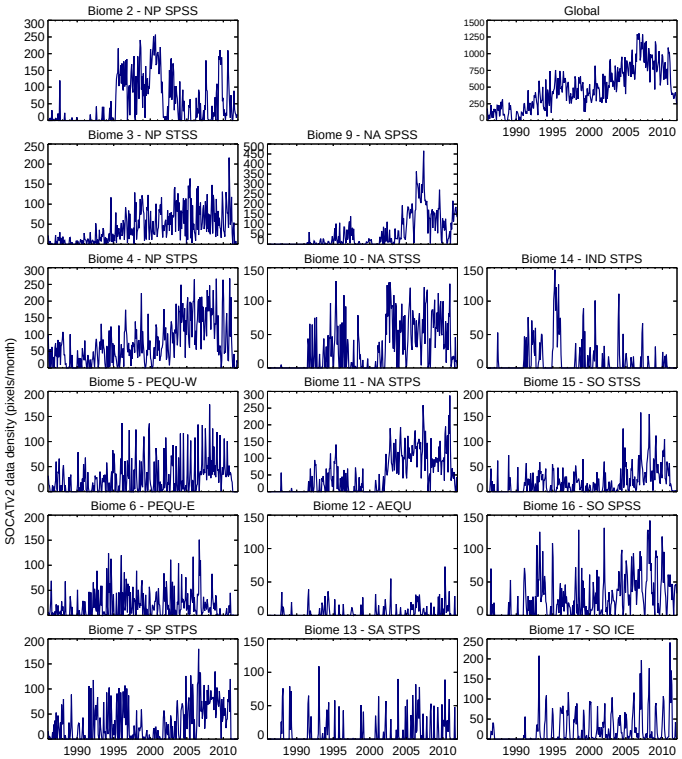

Figure A5. Data density of the gridded SOCATv2 product: number of data-covered pixels per month in each biome. (Note that these values are only roughly indicative of the strength of data constraint, which not only depends on the number of data but also strongly on their distribution within the biome. Also, the magnitudes cannot be compared between biomes, because they have differently many pixels and the pixel size depends on latitude.)

BGD
12, 14049–14104, 2015

An ensemble of pCO_2-based sea–air CO_2 flux estimates

C. Rödenbeck et al.

CC BY

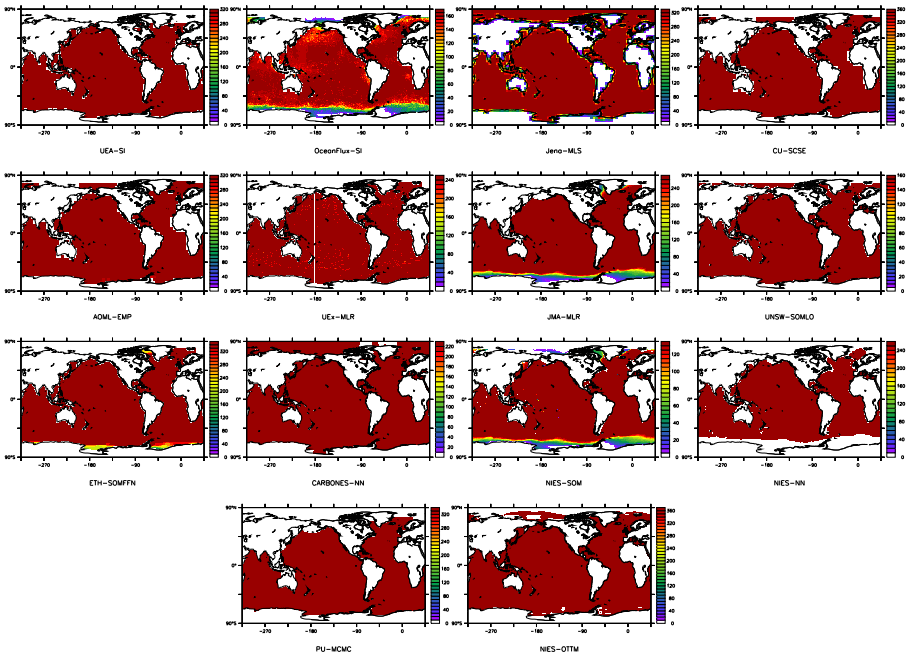

Figure A6. Valid domain for each mapping method (colored area). The color gives the number of valid months within the period of the method; a number less than the maximum (dark red) indicates either (1) a fractional sea mask along coasts (*Jena-MLS*), (2) seasonally invalid months due to unavailable Chlorophyll *a* input data (*JMA-MLR*, *ETH-SOMFFN*, *NIES-SOM*), or (3) occasional invalid months due to other reasons (*OceanFlux-SI*, *UEx-MLR*).

BGD
12, 14049–14104, 2015

CC BY